

Origins of the seasonal variability of PM_{2.5} sources in a rural site in Northern France

P. Espina-Martin^{a,b,*}, E. Perdrix^{a,**}, L.Y. Alleman^a, P. Coddeville^a

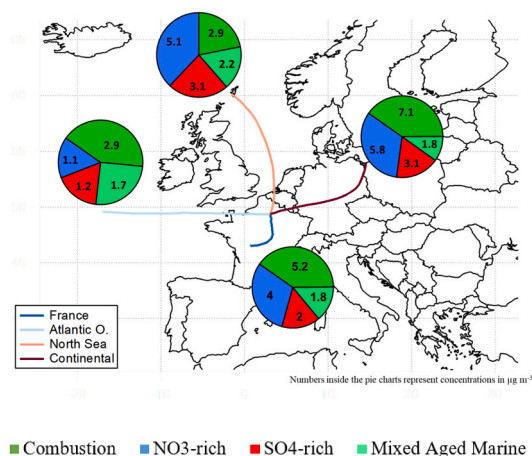
^a IMT Nord Europe, Institut Mines-Télécom, Univ. Lille, Centre for Energy and Environment, F-59000, Lille, France

^b UK Centre for Ecology and Hydrology, Bush State, Penicuik, EH26 0QB, UK

HIGHLIGHTS

- First 1-year study using hourly measurements of precursor gases, water-soluble and carbonaceous aerosols in Northern France.
- High levels of combustion-related aerosols comparable to highly populated areas of NW Europe studies.
- Enhanced NO₃-rich and SO₄-rich transport from Benelux area continues to impact AQ in Northern France.
- NO₃ formation is limited by HNO₃ availability in a NH₃-rich environment.
- PM_{2.5} exposure needs to be addressed both by concentration level and chemical composition.

GRAPHICAL ABSTRACT



ARTICLE INFO

Keywords:

PM_{2.5}
Pollution sources
Positive matrix factorization
Monitor for Aerosols and gases in ambient air (MARGA)
Inorganic precursor gases
Secondary inorganic aerosols (SIA)
Air quality

ABSTRACT

Air quality in rural areas results from the crossing of aged air masses transported from urban areas with local emissions dominated by agriculture and vegetation. The result is a complex mixture of primary and secondary atmospheric species, coming from varied sources and geographical areas. We implemented a methodology for deconvoluting and determining the geographical origins of the main aerosol sources impacting a typical rural area of northern France. A one-year field campaign was conducted in a rural site located between Paris and Brussels from March 2018 to February 2019. Hourly-based observations of inorganic and organic precursor gases and PM_{2.5} speciation were collected using on-line instrumentation. The annual PM_{2.5} concentrations of $12.2 \pm 9.23 \mu\text{g m}^{-3}$ were explained by four sources extracted through positive matrix factorization analyses: combustion (40.2%), NO₃-rich (26.8%), SO₄-rich (18%) and mixed aged marine (15%). The combustion and SIA-rich sources drive 85 % of the yearly PM_{2.5} mass and variability. The combustion factor was most prominent during winter (53.3% of PM_{2.5} mass) due to high contributions from local and regional transport of biomass burning pollutants (winter OC/EC = 6.0; OC-to-OM factor = 2.05). In summer, it was most likely driven by secondary organic

* Corresponding author. IMT Nord Europe, Institut Mines-Télécom, Univ. Lille, Centre for Energy and Environment, F-59000, Lille, France.

** Corresponding author.

E-mail addresses: pabesp@ceh.ac.uk (P. Espina-Martin), esperanza.perdrix@imt-nord-europe.fr (E. Perdrix).

<https://doi.org/10.1016/j.atmosenv.2024.120660>

Received 3 March 2024; Received in revised form 5 June 2024; Accepted 15 June 2024

Available online 15 June 2024

1352-2310/© 2024 The Authors. Published by Elsevier Ltd. This is an open access article under the CC BY license (<http://creativecommons.org/licenses/by/4.0/>).

aerosol production and agricultural waste burning events (summer OC/EC = 8.6; OC-to-OM factor = 1.85). Comparing with other regional sites, we observed a strong regional background of carbonaceous particles regardless of the site typology. The SIA fraction is dominated by the NO₃-rich source compared to the SO₄-rich source. In spring, NO₃-rich particles dominate PM_{2.5} (36.9%) due to intense agricultural activity. The temporal variability is driven by transport processes from the Benelux area in a North-to-South gradient of decreasing concentrations. A minor proportion of the NH₄NO₃ observed seems to be due to the local effects of morning dew and photochemical oxidation of NO₂ in the afternoon. HNO₃ appears to be the limiting factor for local NH₄NO₃ formation. PM_{2.5} toxicity in rural areas with low population densities should be not only addressed based on mass concentration, but also considering the chemical composition of particles as people from rural environments are exposed to high contributions from biomass burning sources and secondary inorganic aerosols triggered by the NH₃ excess.

List of abbreviations

BVOC	Biogenic Volatile Organic Compound	NWR	Non-Parametric Wind Regression
BSOA	Biogenic Secondary Organic Aerosols	OC	Organic Carbon
C-C	Caillouël-Crépigny	OM	Organic Matter
EC	Elemental Carbon	PBL	Planetary Boundary Layer
F _{OC-OM}	Factor of conversion of OC to OM	PAH	PolyAromatic Hydrocarbons
FA	Factor Analysis	PM _{2.5}	Particulate Matter ≤2.5 μm
FDMS	Filter Dynamics Measurement System	PMF	Positive Matrix Factorization
GC-FID	Gas Chromatographic - Flame Ionization Detector	PSCF	Potential Source Contribution Function
HdF	Hauts-de-France, France's northernmost administrative region	QA/QC	Quality Control/Quality Assurance
HYSPLIT	HYbrid Single-Particle Lagrangian Integrated Trajectory	RH	Relative Humidity
IC	Ionic Chromatography	RM	Remaining Mass
LOD	Limit of Detection	S/N	Signal-to-Noise ratio
LRT	Long Range Transport	SIA	Secondary Inorganic Aerosols
MAM	Mixed aged marine factor	SOA	Secondary Organic Aerosols
MARGA	Monitor for AeRosols and Gases in ambient Air	TD	Thermal Desorption
		TEOM	Tapered Element Oscillation Microbalance
		UTC	Coordinated Universal Time

1. Introduction

Air pollution is currently the most important environmental risk to human health and is perceived as the second biggest environmental concern after climate change for the European population (European Commission, 2019). Among atmospheric pollutants, fine particulate matter (PM_{2.5}) is one of the most hazardous over human health, as only in Europe, 307,000 premature deaths were attributed to chronic exposure of PM_{2.5} (EEA, 2021). Furthermore, it is one of the most complex due to its heterogeneous nature and multiple sources. Depending on the origins of the particles' constituents, they can be classified as primary if directly emitted, or secondary if they are formed through physico-chemical processes in the atmosphere from precursor gases.

Recent studies conducted in the European area have shown that the PM_{2.5} hotspots are located in Southern Poland, the Po Valley (Italy) and, to a lesser degree, the areas of Benelux and Northern France (Bigi and Ghermandi, 2016; EEA, 2021; Kobza et al., 2018). Although the PM_{2.5} concentrations are lower compared to Polish or Italian sites, Benelux and Northern France are densely populated areas (Koceva et al., 2016) with significant agricultural and livestock activities and high residential, industrial and power plants sources that induce high emission levels of NO_x and on a lesser scale, SO₂ (EEA, 2021; Gauss et al., 2019). Both gases are precursors of secondary inorganic particles (SIA), as they can be oxidized through photochemical processes to produce HNO₃ and H₂SO₄, respectively. These acids are neutralized with NH₃, mainly emitted by agricultural sources such as animal excretions or synthetic fertilizers (Paulot et al., 2014) to produce ammonium sulfate and ammonium nitrate (Hauglustaine et al., 2014; Seinfeld and Pandis, 2016). Benelux and Northern France areas are hotspots for NH₃ emissions, due to the intensive agriculture activity practised here (Drugé

et al., 2019). This results in SIA accounting up to 60% of PM_{2.5} mass in Northwest Europe, as evidenced by past studies conducted in this area (Mooibroek et al., 2011; Putaud et al., 2010). In Northern France, even though the flat topography should favour the dispersion of pollutants, recurrent high PM_{2.5} episodes occur during winter and spring seasons (Roig Rodelas et al., 2019b; Schaap et al., 2011). These events have been linked to transboundary continental air masses coming from Benelux, Eastern Europe, the Channel and the North Sea (Potier et al., 2019; Waked et al., 2014), resulting in PM_{2.5} annual values between 10 and 20 μg m⁻³, above the World Health Organization (WHO) recommended value of 5 μg m⁻³, reducing the people's life expectancy in this area between 6 and 8 months (Pascal et al., 2013).

Previous studies on the sources of PM in the North of France (Hauts-de-France Region) have been focusing on the metal source apportionment and their size distribution on the coarse fraction (Alleman et al., 2010; Mbengue et al., 2014), or have determined the chemical composition and source apportionment of the fine particles using offline-based methodologies (Ledoux et al., 2017) or continuous instrumentation during intensive short periods of time (Crenn et al., 2017, 2018). These studies highlight the prevalence of NH₄NO₃ and (NH₄)₂SO₄ in PM_{2.5} composition, representing more than 50% of the total aerosol mass, a trend observed in other Northwestern European sites (Putaud et al., 2010). Only one 1-year long field campaign using online instrumentation was conducted in the region at a suburban site of the city of Douai (Roig Rodelas et al., 2019b), which focused on the origins and processes governing the predominant SIA fraction by measuring both inorganic precursor gases and aerosols on an hourly basis using a MARGA (Makkonen et al., 2012; Twigg et al., 2015), allowing to better understand the temporal variability and the geographical origins of the inorganic gas precursors and PM_{2.5} speciation. Nonetheless, there was a lack of information on the sources and levels of PM_{2.5} affecting the rural

environments where the main agricultural sources are located.

The air quality in rural areas has generally been considered healthier than in urban areas because of lower primary anthropogenic emissions, coupled with the higher dispersion and the lack of the “heat island” effect (Harrison, 2018). However, agricultural sources (fertilizers, biomass burning, dust, phytosanitary products) and the potential different atmospheric chemical regime in rural areas (lower NO_x and SO₂ but higher NH₃, O₃ and biogenic volatile organic compounds (BVOCs)) generally in opposition to urban ones may influence local air quality and, more specifically SIA formation. Atmospheric oxidative capacity differs between urban and rural sites, as some studies suggest the predominance of O₃-based chemistry for OH production in rural sites, whereas urban sites are more dominated by the photolysis of HONO (Atkinson and Aschmann, 1993; Harrison et al., 2006; Heard et al., 2004). Previous source apportionment studies have been conducted in the region, although none of them was performed in rural site and dedicated to the PM_{2.5} fraction. Therefore, this manuscript aims to present the results of a 1-year field campaign with a hourly time resolution conducted in a rural site located in the North of France using similar instrumentation as in (Roig Rodelas et al., 2019b) complemented with an online organic carbon and elemental carbon (OC-EC) analyser to get the PM_{2.5} mass closure, and with an online VOC analyser to monitor BVOCs. The objectives are to (i) characterize the sources of fine particulate pollution in this area, (ii) determine the geographical origin of the precursor gases and PM_{2.5} sources and (iii) explain the main drivers and processes of the PM_{2.5} pollution.

2. Materials and methods

2.1. Campaign description

Hourly observations of inorganic gas precursors, PM_{2.5} mass and chemical speciation were conducted from March 01, 2018 until February 28, 2019 in Caillouël-Crépigny (C-C) (447 inhab; 49° 37' 11.4" N, 3° 7' 36.5" E, 95 m a.s.l.; (INSEE, 2019, Fig. 1). The site is 5 km away from big urban and industrial sources and it is exposed to mixed influences from surrounding agricultural fields, forested areas, and nearest scarce population areas. Several industries are located within a 40 km radius, mostly chemical factories, sugar refineries and glass workshops (Table S1, Fig. S1). The landscape in this area is mostly flat, with almost no obstacles favouring the dispersion of pollutants. The climate is characterized as temperate oceanic, with low seasonal amplitudes and regular precipitation regime over the year.

2.2. Instrumentation

The MARGA 1S – ADI 2080 (Metrohm Applikon, Schiedam, Netherlands) was deployed to obtain simultaneous hourly

concentrations of 8 inorganic water-soluble aerosol species (NO₃⁻, SO₄²⁻, Cl⁻, Ca²⁺, Mg²⁺, Na⁺, K⁺, NH₄⁺) and 5 inorganic precursor gases (HCl, HNO₃, HONO, SO₂, NH₃) with 1-h time resolution. Details on the MARGA functioning principle can be found elsewhere (Espina-Martin et al., 2022; Roig Rodelas et al., 2019b). Outdoor air is pumped at a flowrate of 1 m³ h⁻¹ through a Teflon-coated PM_{2.5} sampling head (Sven Leckel, Berlin, Germany) connected to the Sample box by a 1.3 m long polyethylene tube (outer \varnothing = 1.27 cm) isolated to prevent condensation inside the tube. The sample analysis was conducted by means of ionic chromatography (IC) coupled with conductivity detection. Both cation and anion systems inject the samples through fixed loops of 500 μ L and 250 μ L, respectively. A Metrosep C4 100 \times 4 mm column was used for anions and a Metrosep A Supp10-75 for cations (Metrohm-Applikon, Schiedam, Netherlands). Both columns were inside an oven maintaining their temperature around 40 \pm 5 °C. The anion IC uses an eluent of 7 mM Na₂CO₃ with 8 mM NaHCO₃, sample mixed with the eluent through a suppressor module regenerated with phosphoric acid (H₃PO₄) before heading into a conductivity meter. For the cation IC, an aqueous solution of 3.2 mM p-toluene sulfonate was used. The limit of detection (LOD) of the species are in Table S2. A Semi Continuous OC-EC Field Analyzer Model 4 (Sunset Laboratory Inc., USA) (Bauer et al., 2009) was used to perform 1-h measurements of OC and EC from PM_{2.5} using the analytical protocol from the European Supersites for Atmospheric Aerosol Research (EUSAAR-2), based on thermal optical transmittance (TOT) composed of two successive steps (Birch and Cary, 1996; Cavalli et al., 2010). Total PM_{2.5} mass was measured using a Tapered Element Oscillation Microbalance (TEOM) 1405-F (ThermoFischer) with Filter Dynamics Measurement System (FDMS) at hourly time resolution. Nitrogen oxides were analyzed every 15 min with a chemiluminescent analyzer NO_x M200 EH/EM (Envirocontrol, Teledyne). Isoprene measurements were acquired using a TurboMatrix Thermal Desorption (TD) unit coupled to a Clarus 580 Gas Chromatographic (GC) (PerkinElmer) system with a flame ionization detector (FID). The TD allows to pre-concentrate the target VOCs via an adsorbent trap cooled down at 10 °C by a Peltier system. Further information on the data quality control and assurance protocols (QA/QC) for all instruments can be found in Table S3. Temperature, relative humidity (RH), wind speed & direction datasets were provided by a local meteorological station, while the closest MeteoFrance stations provided hourly information for the rain (Chauny, 5 km E), global radiation and atmospheric pressure (Saint Quentin, 22.5 km NE). All presented measurements are given in Coordinated Universal Time (UTC), and seasons are differentiated as follows: winter (December, January, February), spring (March, April, May), summer (June, July, August) and autumn (September, October, November).

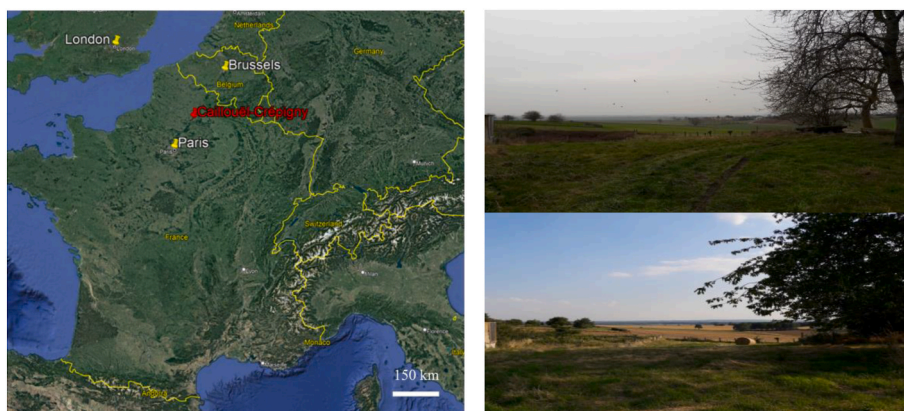


Fig. 1. Location map of the study site in the North of France (left) and views of the rural area of Caillouël-Crépigny at different seasons (right).

2.3. Source apportionment of PM_{2.5}

A Positive Matrix Factorization (PMF) analysis was conducted on the 1-year database to determine which were the main sources influencing PM_{2.5} using the EPA PMF 5.0 software (Bressi et al., 2014; Paatero and Tapper, 1994; Ulbrich et al., 2009). The two input datasets required for the PMF analysis (for concentrations and their associated uncertainties) only considered the hours with all species measured correctly, representing more than 5500 h in the final dataset. The uncertainty dataset for the MARGA species was calculated based on the methodology presented in Espina-Martin et al. (2022), where each species have their uncertainties calculated based on an hourly basis depending on their proximity to their LOD, the repeatability and representativeness of the species measurement, and the fluctuations on parameters such as the air volume, liquid sample volume injected in the IC, IS quality. For the Semi Continuous OC-EC analyzer and TEOM-FDMS, the measurements uncertainties were calculated using the expanded relative uncertainties values used by previous authors; for OC an uncertainty of 10% was applied (Lim et al., 2003; Waked et al., 2014), while EC uncertainty was set to 15% (Cavalli et al., 2010; Schmid et al., 2001). Finally, PM_{2.5} mass concentration uncertainty was set to 20% (Aymoz and Mathé, 2007). Concentrations under the limit of detection (LOD) were substituted by 1/2 LOD for the species and their uncertainty was assigned to 100%, in order to down weight their influence on the final solution (Norris et al., 2014). An additional 10% of uncertainty was introduced into the model to include unaccounted error sources. Prior to the PMF analysis, a Varimax-rotated factor analysis (FA) was performed on the aerosol species dataset to estimate the possible number of factors and see the correlations between the aerosol species and PM_{2.5} using the software STATGRAPHICS Centurion XV. II.

2.4. Geographic origin of the sources

Non-Parametric Wind Regression (NWR) and Potential Source Contribution Function (PSCF) analyses were used using ZeFir IGOR tool v 3.7 (Petit et al., 2017b) to determine the most probable geographic origins of the extracted sources. The NWR analysis was used to locate and to estimate the possible local sources of a pollutant as it combines pollutant concentrations with local wind speed and direction (Henry et al., 2009). To determine the origins of the sources possibly linked to long-range transport (LRT), PSCF was used to backtrack and determine the most probable regions of emissions for the gaseous and particulate species. It requires the use of back trajectories calculated with HYSPLIT 4 (HYbrid Single-Particle Lagrangian Integrated Trajectory; Stein et al., 2015), for an arrival height of half the mixing layer to take into account the temporal variation of the planetary boundary layer (PBL) at a 3-h interval, 72 h back in time; more information on the seasonal variation of the PBL can be found in Table S4. The extracted trajectories were used for both a cluster analysis and to generate the PSCF maps. The PSCF was constrained following the approach of similar studies by eliminating back-trajectories when considering the effect of wet scavenging whenever the air mass passes over an area with precipitations (>1 mm h⁻¹ (Kim et al., 2014; Waked et al., 2018),) or if it goes above the maximum height of the PBL found in the HYSPLIT meteorological file (1500 m; Roig Rodelas et al., 2019b).

3. Results

3.1. Overview of the campaign and PM_{2.5} composition

Table 1 shows the main statistics of the measured species during the campaign. All inorganic gases (except HCl), PM_{2.5}, SIA species and OC and EC were consistently over the LOD, while HCl, NO, Cl⁻, Na⁺, Ca²⁺, Mg²⁺ and K⁺ were mostly under their LOD. PM_{2.5} annual average and standard deviation from hourly data were 12.2 ± 9.23 μg m⁻³, with half of the PM_{2.5} mass driven by NO₃⁻, SO₄²⁻, NH₄⁺, accounting for 27%, 14%

and 10%, respectively. (Fig. 2). The rest of the aerosol mass was composed of the carbonaceous species representing 24% (20% OC, 4% EC), and 3% of the minor ions sum (Cl⁻, Na⁺, K⁺, Mg²⁺, Ca²⁺). The remaining unspiciated fraction accounted for chemicals elements bound to OC to form organic matter (OM) and insoluble minerals. Indeed, as explained in section 5 of the Supplement, it was estimated that OM accounted for 33% of the annual PM_{2.5}, thus reducing the unspiciated fraction to 9%. The minor ions data collection was limited either due to occasional marine events (Cl⁻, Na⁺) or to the low sensitivity of the MARGA, preventing the correct measurement of these species. The ions Cl⁻ and Na⁺ are marine-related species and do correlate for all seasons, especially during winter (r = 0.64), when marine air masses arrived more frequently at our site.

$$\text{TEOM PM}_{2.5} = 12.2 \pm 9.23 \mu\text{g m}^{-3}$$

The seasonal OC/EC mass ratios are 5.7, 8.6, 5.2, 6.0 respectively for spring, summer, autumn and winter, with higher values occurring in winter (6.0) most likely due to high biomass burning Mbengue et al., 2018), and summer (8.6) when high levels of isoprene and photochemical activity are ongoing contributing to secondary organic aerosol (SOA) formation (Waked et al., 2016). Isoprene concentrations were under LOD from October to April, while reaching their peak during July and August (Fig. S2). High pollution episodes (PM_{2.5} > 25 μg m⁻³) occurred at all seasons as seen in Fig. S3. Spring and autumn had the highest frequency of occurrence with 10 and 9 episodes, respectively. These episodes were most likely consequence of the intense agricultural activity occurring in Northwest Europe during these months, increasing the airborne concentrations of NO₃⁻ and NH₄⁺ and, on a minor scale, SO₄²⁻. On the contrary, during winter there were 6 high PM_{2.5} episodes, half of them caused by high loads of carbonaceous aerosols released from combustion processes occurring from October until April, coinciding with the cold period (Table S4).

3.2. FA and PMF results

3.2.1. Source apportionment optimization

Prior to the source apportionment analysis, a FA was carried out to screen the optimal number of factors to be input in the PMF. More than six thousand observations (Table S5) were used in the FA and four factors were extracted with eigenvalues superior to 1 (Fig. S4, Table S6).

- FA-Factor 1: NO₃⁻, NH₄⁺ and SO₄²⁻. This factor contains all SIA species, representing secondary inorganic aerosols.
- FA-Factor 2: OC, EC, and K⁺: This factor represents combustion processes such as traffic-related fuel combustion or biomass burning.
- FA-Factor 3: Cl⁻, Na⁺, and Mg²⁺: These species are related to marine sources.
- FA-Factor 4: Ca²⁺ and Mg²⁺: This factor represents the crustal source most likely from the agricultural fields surrounding the site.

Although the FA suggested an optimal number of factors equal to 4, the PMF analysis can separate some of these factors based on their distinctive temporal patterns and appliance of constrains over specific tracers. For example, FA-Factor 1 combines both NO₃-rich and SO₄-rich SIA sources, however previous studies conducted on the region (Mooibroek et al., 2011; Bressi et al., 2014; Roig Rodelas et al., 2019a) had separated them successfully into NO₃-rich and SO₄-rich sources without applying constrains to their modelling since both sources have distinctive temporal patterns and geographical origins, hence a potential 5 factor solution was considered for the PMF analysis based on the results of the FA and previous knowledge of the region.

For the PMF analysis, more than 5500 observations were used for the PMF analysis (Table S7). Table 2 shows the main statistics of the database, as well as the categorization of the species as strong, weak, or bad based on their signal-to-noise ratio (S/N), the confidence in the quality

Table 1

Statistical summary of measured species in Caillouël – Crépigny.

The amount of data above the limit of detection ($n > \text{LOD}$) is expressed in %; average (Avg), standard deviation (Std) and 2.5th, 50th and 97.5th percentiles are expressed in $\mu\text{g m}^{-3}$.

	Spring					Summer					Autumn					Winter				
	n > LOD (%)	Avg.± Std	P _{2.5}	P ₅₀	P _{97.5}	n > LOD (%)	Avg.± Std	P _{2.5}	P ₅₀	P _{97.5}	n > LOD (%)	Avg.± Std	P _{2.5}	P ₅₀	P _{97.5}	n > LOD (%)	Avg.± Std	P _{2.5}	P ₅₀	P _{97.5}
HCl	0.0	<LOD	<LD	<LD	<LD	0.4	<LD	<LD	<LD	<LD	0.2	<LD	<LD	<LD	<LD	1.2	<LD	<LD	<LD	<LD
NO	23.7	1.27 ± 1.92	<LD	0.86	5.59	11.1	0.65 ± 1.2	-0.78	0.32	3.76	28.9	2.25 ± 3.78	<LD	<LD	24.54	26.7	2.53 ± 5.76	<LD	<LD	15.15
NO ₂	89.9	8.77 ± 4.34	<LD	8.08	19.12	79.1	5.4 ± 3.24	0.78	4.9	12.45	89.6	8.44 ± 5.8	4.48	7.16	24.54	82.1	11.26 ± 10.13	<LD	8.5	36.83
O ₃	94.8	66.1 ± 22.2	32.48	64.9	116	100	71.29 ± 32.1	23.53	65.2	143.30	97.7	44.12 ± 21.9	28.08	43.33	92.52	94.5	44.45 ± 19.59	7.06	47.12	76.38
HONO	78.2	0.76 ± 0.45	<LD	0.69	1.55	84.5	0.6 ± 0.35	<LD	0.54	1.41	86.5	0.75 ± 0.43	0.47	0.7	1.8	77.9	0.82 ± 0.76	<LD	0.62	2.81
HNO ₃	64	0.25 ± 0.24	<LD	0.21	0.85	71.7	0.36 ± 0.27	<LD	0.34	0.94	54.2	0.16 ± 0.16	<LD	0.12	0.5	44.8	0.13 ± 0.28	<LD	<LD	0.48
SO ₂	81.4	0.53 ± 0.45	0.13	0.38	1.84	88.1	0.76 ± 0.72	0.13	0.53	2.81	85.4	0.54 ± 0.47	0.26	0.41	1.79	78.6	0.37 ± 0.31	<LD	0.29	1.18
NH ₃	81.8	5.17 ± 3.69	0.61	4.43	15.46	87.7	4.55 ± 2.6	1.13	4.06	11.65	87.9	2.94 ± 1.57	1.94	2.75	6.04	68.9	3.06 ± 4.12	0.54	1.6	16.05
Cl ⁻	10.0	0.11 ± 0.37	<LD	<LD	1.24	5.1	0.03 ± 0.15	0	<LD	0.49	10.4	0.05 ± 0.19	<LD	<LD	0.54	15.3	0.13 ± 0.46	<LD	<LD	1.87
NO ₃ ⁻	78.8	4.42 ± 5.16	0.42	2.48	19.54	86.3	2.2 ± 3.28	0.09	0.94	13.63	84.9	3.24 ± 4.02	0.77	1.47	14.47	85	2.82 ± 3.26	0.1	1.61	13.19
SO ₄ ²⁻	79.4	1.72 ± 1.31	0.43	1.34	5.48	88.3	2.12 ± 1.7	0.41	1.67	7.06	86.3	1.84 ± 1.52	0.86	1.34	5.98	86.3	0.9 ± 0.61	0.18	0.76	2.48
Na ⁺	13.8	0.04 ± 0.1	<LD	<LD	0.35	22.3	0.06 ± 0.09	0	0.03	0.35	47.2	0.12 ± 0.15	<LD	0.08	0.56	25.5	0.13 ± 0.28	<LD	<LD	0.88
NH ₄ ⁺	74.0	1.31 ± 1.78	<LD	0.59	6.88	87	1.09 ± 1.35	0.07	0.61	5.43	88	1.51 ± 1.62	0.4	0.83	5.7	30.1	1.04 ± 1.16	0.08	0.59	4.55
K ⁺	16	0.07 ± 0.08	<LD	<LD	0.26	18.9	0.09 ± 0.1	0	0.07	0.34	27.1	0.11 ± 0.1	<LD	<LD	0.4	87.5	0.12 ± 0.11	<LD	<LD	0.39
Mg ²⁺	7.8	0.04 ± 0.03	<LD	<LD	0.11	2.4	0.03 ± 0.02	0	0.03	0.08	5.4	0.09 ± 0.07	<LD	<LD	0.11	29.1	0.04 ± 0.04	<LD	<LD	0.12
Ca ²⁺	17.2	0.12 ± 0.11	<LD	<LD	0.42	20.4	0.12 ± 0.15	0	0.07	0.52	10.4	0.09 ± 0.07	<LD	<LD	0.29	7.4	0.08 ± 0.06	<LD	<LD	0.21
OC	77.3	2.95 ± 2.28	0.75	2.34	9.32	83.4	1.8 ± 0.96	0.5	1.57	3.88	91.3	2.53 ± 2.18	1.23	1.84	8.17	7.1	2.8 ± 2.8	<LD	1.85	10.62
EC	73.6	0.52 ± 0.46	<LD	0.37	1.78	68.2	0.21 ± 0.18	0	0.18	0.58	75.3	0.49 ± 0.52	0.15	0.34	1.82	73.7	0.47 ± 0.59	<LD	0.28	1.93
Isoprene	22.2	0.07 ± 0.16	<LD	<LD	0.42	88.1	0.45 ± 1.05	<LD	0.2	1.86	28.7	0.12 ± 0.52	<LD	<LD	0.5	15.8	0.04 ± 0.05	<LD	<LD	0.17
PM _{2.5}	89.1	13.73 ± 10.6	<LD	10.51	40.93	91.2	9.49 ± 7.96	0.98	7.5	33.60	71	12.19 ± 8.97	<LD	9.40	34.55	58.5	14.55 ± 10.94	<LD	11.56	41.46

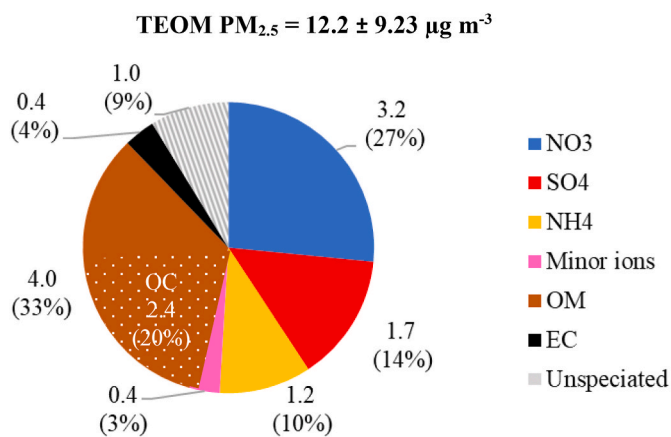


Fig. 2. Annual average composition of PM_{2.5} in C-C during the 1-year campaign.

Table 2
Percentiles, S/N and LODs of the variables used as inputs for the PMF.
All concentrations are expressed in µg m⁻³.

Variable	S/N	Category	Min	25th	Median	75th	Max	½ LOD
Cl ⁻	0.7	Strong	0.015	0.015	0.015	0.015	3.6	0.015
NO ₃ ⁻	8.5	Strong	0.035	0.69	1.4	3.7	36.3	0.035
SO ₄ ²⁻	9.7	Strong	0.02	0.79	1.3	2.1	14.1	0.02
Na ⁺	0.4	Strong	0.035	0.035	0.035	0.095	1.5	0.035
NH ₄ ⁺	5.6	Strong	0.025	0.30	0.63	1.4	12.3	0.025
K ⁺	0.1	Weak	0.070	0.070	0.078	0.14	0.78	0.07
Mg ²⁺	0.1	Weak	0.040	0.040	0.040	0.05	0.21	0.04
Ca ²⁺	0.1	Bad	0.075	0.075	0.075	0.11	2.3	0.075
OC	3.4	Strong	0.25	1.1	1.86	3.0	29.7	0.25
EC	1.7	Strong	0.025	0.12	0.27	0.54	6.60	0.025
PM _{2.5}	4.3	Weak*	1	5.4	9.04	15.47	62.9	1

PM_{2.5} is the total variable, and thus automatically categorized as weak.

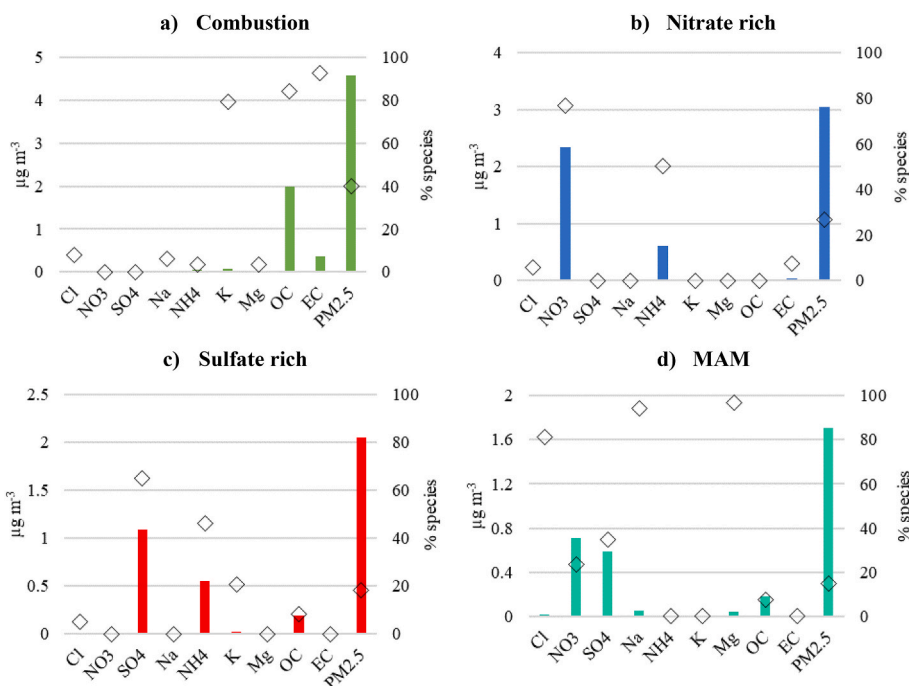


Fig. 3. Chemical profiles of the 4-factor solution.

of the tracer analysis, and their representativeness towards the final solution.

The SIA, OC and EC species S/N ratios were close or over 2 and were categorized as strong variables. Cl⁻, Na⁺, Mg²⁺ and K⁺ ions had S/N ratios of 0.7, 0.4, 0.1 and 0.1 respectively, categorizing them either as weak or bad variables. Based on the results of the FA, Cl⁻ and Na⁺ were kept as strong variables with Mg²⁺ as a weak variable to extract the FA-Factor 3 related to marine sources, while K⁺ was kept as a weak variable to help extracting FA-Factor 2, related to combustion processes. Ca²⁺ was used as a weak tracer to help pull out the FA-Factor 4 related to crustal sources, however the 5-factor solution in the PMF was unsuccessful in extracting the crustal source as Ca²⁺ S/N is too low to reliably represent this source and the 5-factor solution did not have a physical meaning nor environmental sense. The final PMF solution excluded Ca²⁺ and a 4-factor was chosen, based on the good Q_{true}/Q_{expected} value (1.4), on the physical meaning of the chemical profiles and their time variability, and the good correlations between observed and modelled species of the PM_{2.5}.

3.2.2. PMF results

All strong species but EC, Cl⁻ and Na⁺ were modelled satisfactorily with “model versus observation” slopes close to 1 and R² ≥ 0.9. The EC

regression values were still good, with a slope of 0.69 and $R^2 = 0.77$ (Table S8), however they indicate a decrease in the model goodness of fit. This is possibly due to sporadic local events of crop biomass burning, different from the usual EC sources related to traffic and domestic heating. The marine events were scarcer compared to the other strong variables over the year and thus the model did not perform well replicating the temporal variability of the marine tracers.

Fig. 3 shows the chemical profiles of the four extracted factors, indicating the % and mass concentration in $\mu\text{g m}^{-3}$ for each species. This solution was considered to be stable as the sum of the mass of the 4 identified factors and the gravimetric mass of $\text{PM}_{2.5}$ had a good correlation ($R^2 = 0.85$, slope = 0.9).

The concentrations are expressed as solid bars (left axis) and the % of species concentration as diamonds (right axis)

- **Combustion:** Representing the carbonaceous aerosols, it is driven by high % species contribution from OC (84.1%), EC (92.5%) and K^+ (79.4%) (Fig. 3a). The sum of OC and EC represent about 95% of the factor mass, while the 5% remaining is composed of K^+ and NH_4^+ . On an annual basis, this factor is strongly correlated to both OC and EC ($R^2 = 0.89$ and 0.77).
- **NO_3 -rich:** The major contributors are NO_3^- (76.7%) and NH_4^+ (50.3%), representing 90.4% of the factor mass, and the rest comes from EC (Fig. 3b). It is highly correlated with NO_3^- and NH_4^+ ($R^2 = 0.99$ and 0.94, respectively).
- **SO_4 -rich:** Driven by SO_4^{2-} (65%), NH_4^+ (46.2%) and K^+ (20.6%), the residual % of species are OC (8.3%) and Cl^- (4.9%) (Fig. 3c). 80.5% of the factor mass is composed of SO_4^{2-} (65%) and NH_4^+ , most likely in the form of $(\text{NH}_4)_2\text{xH}_2\text{SO}_4$. It is highly correlated with SO_4^{2-} and NH_4^+ (0.93 and 0.62, respectively)

Mixed aged marine factor (MAM): The fourth factor was identified as mixed aged marine sources, driven by Cl^- (81.4%), Na^+ (94.1%) and Mg^{2+} (96.7%), with lesser species contributions of NO_3^- (23.4%), SO_4^{2-} (35%) and OC (7.6%) (Fig. 3d). Although the factor is driven by the marine tracers, the majority of the mass is made up of NO_3^- and SO_4^{2-} , therefore its mixed status. This prevalence of secondary aerosols is consistent with the assumption of aged air masses as the C-C site is 130 km away from the sea in a straight line.

All factors were stable except the MAM, which was mixed with the sulfate-rich factor as seen in the bootstrap analysis (Table S9). To better separate this MAM factor, a constrain was performed and Na^+ , Cl^- and Mg^{2+} were maximally pulled up while minimizing OC, EC, and K^+ contributions in this factor. This configuration allowed to completely differentiate all the factors. The constrained solution increased the % of species for all marine tracers by $\geq 10\%$ in the marine factor, while OC, EC, and K^+ increased by 10%, 9% and 45% respectively in the combustion factor source (Fig. S5).

Fig. 4 shows the absolute and relative contributions of the four

extracted sources towards $\text{PM}_{2.5}$ mass on a seasonal and annual level. On an annual basis and from highest to lowest contribution, the combustion factor is the single largest contributor out of all the identified sources towards the $\text{PM}_{2.5}$ (40.2%), followed by the NO_3 -rich (26.8%), SO_4 -rich (18%), and MAM factor (15%). The sum of the secondary sources is indeed the largest contributor towards the annual $\text{PM}_{2.5}$ mass (44.8%), while the MAM factor is consistently the lowest contributor towards fine PM on a seasonal basis.

4. Discussion

The extracted factors were interpreted based on their chemical profile, geographical origin determined by means of NWR and PSCF analysis, correlation with other tracers and temporal (seasonal daily, monthly) variability. Although the combustion factor is the single largest contributor of $\text{PM}_{2.5}$, the two secondary factors are the major drivers of the fine particles at C-C (44.8 %). In the next subsections we will discuss the drivers of the temporal variability for the extracted factors (Fig. 5).

4.1. Combustion and summer BSOA

The combustion factor is characterized by a high OC/EC ratio of 5.4, and OC (84.1%), EC (92.5%) and K^+ (79.4%) driving the chemical profile, pointing to biomass burning as the main combustion process in C-C (Andersen et al., 2007; Mbengue et al., 2018). It is likely that minor traffic sources also impacted the C-C site, as there are two highways located in the West and East sectors 20–25 km away from C-C, and a departmental road less than 10 km to the South (Fig. S1), however on an annual basis, the combustion factor is weakly correlated to NO , NO_2 and HONO ($R^2 = 0.18$, 0.27, and 0.36, respectively), and the lack of availability of information on other combustion tracers such as levoglucosan, Mn, Fe, Cu, and Ni, associated with biomass burning and non-exhaust vehicular emissions (Schauer et al., 2006; Thorpe and Harrison, 2008) prevented the further separation of this factor. This factor has a high seasonal variability, contributing 53.3% of the $\text{PM}_{2.5}$ mass during winter while decreasing to 28.7% in summer (Fig. 4b). Fig. 5 shows how after May the concentrations decrease with the warm season until September. All diel seasonal profiles except summer have two peaks, a small one in the morning (8:00–12:00) and a more intense one during the evening (19:00–21:00), coincident with the traffic rush hours but most of all with the activation of household heating devices. During summer, heating systems are off and the potential contribution of traffic diminishes due to the summer holiday period (Mooibroek et al., 2011). However, the July average concentration increases compared to other summer months. This increase could match agricultural waste burning events spotted in the surrounding agricultural fields after the reaping of crops. The summer K^+ NWR plot shows moderate local signals of $0.15 \mu\text{g m}^{-3}$, reflecting the occurrence of these events (Fig. S11e).

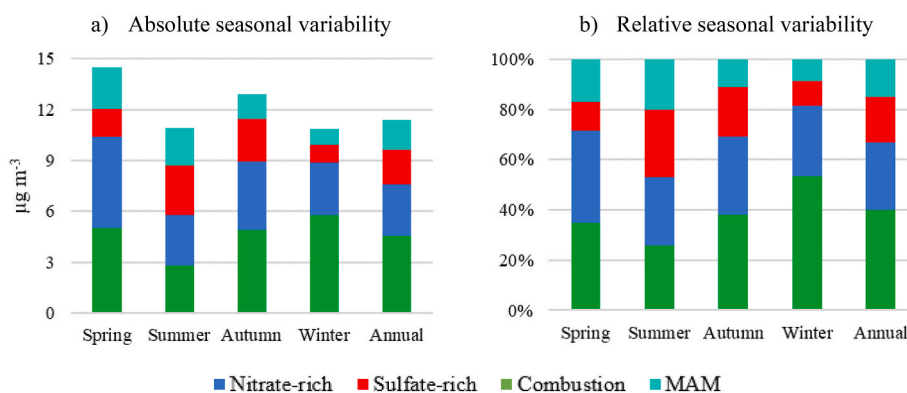


Fig. 4. Seasonal absolute and relative contribution of the PMF sources towards $\text{PM}_{2.5}$ in C-C.

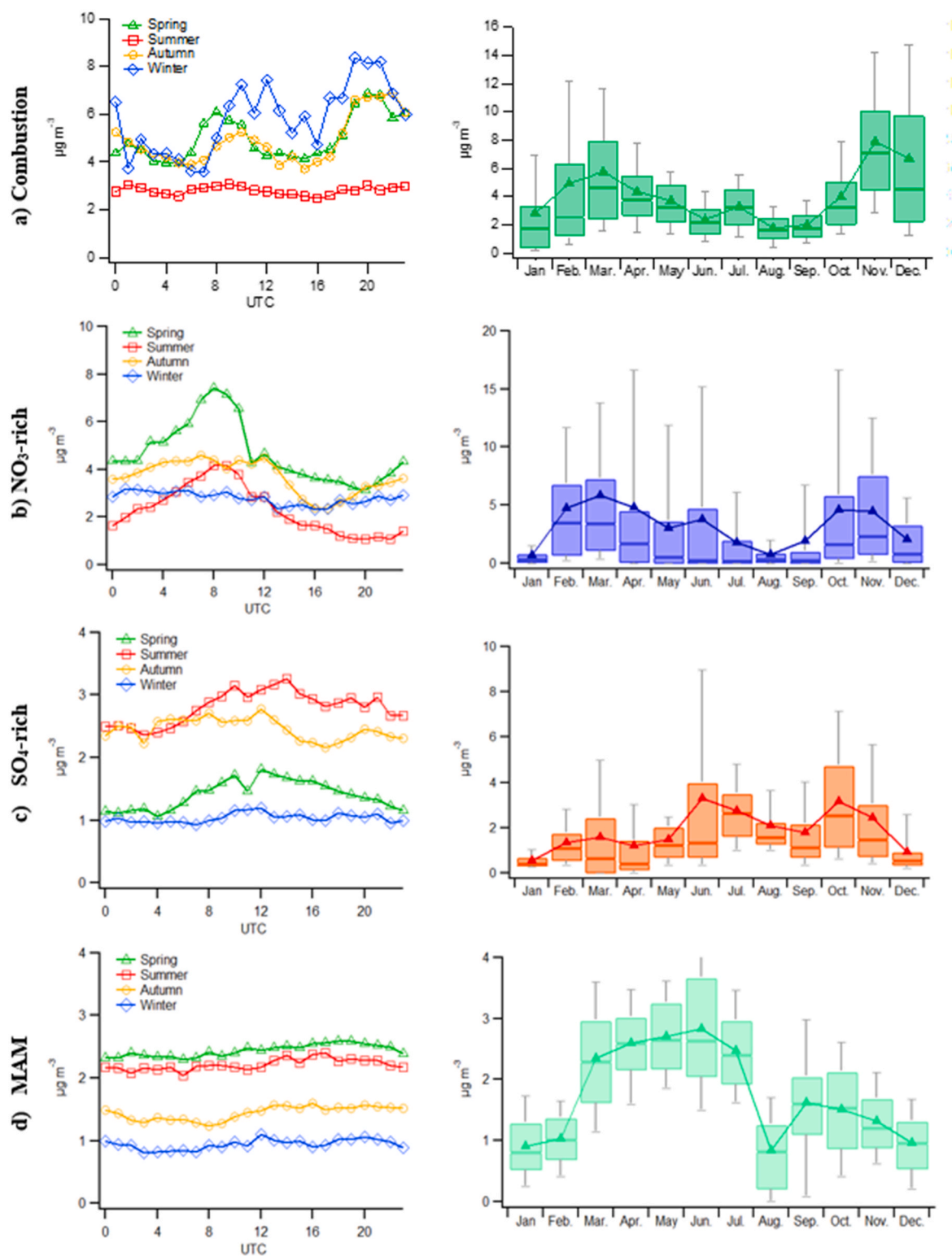


Fig. 5. Seasonal (left) and monthly (right) temporal variability of the PMF factors for the 1-year campaign.

Additionally, July 2018 was one of the hottest months in the history of France (Meteo France, 2022), with monthly averages of $T = 22.3 \pm 4.4$ °C, $O_3 = 85.5 \pm 33.3$ $\mu\text{g m}^{-3}$ and wind speed = 1.4 ± 0.8 m s^{-1} , promoting a highly oxidative atmosphere with low pollutant dispersion. Although the scope of this paper is not the quantification of biogenic secondary organic aerosols (BSOA), the high local isoprene concentrations up to 4 ppb (Fig. S2), the local OC NWR signal in summer

(Fig. S10d) and the high OC/EC ratio (8–12) observed during summer afternoons (Fig. S6) hinted at potential BSOA formation contributing towards the carbonaceous aerosol fraction. This was further strengthened when the factor of conversion of OC to organic matter (OM), $F_{\text{OC-OM}}$, was estimated for each season, following a published method by Bressi et al. (2013). The method estimates the $F_{\text{OC-OM}}$ based on the OC fraction and the remaining mass (RM, calculated by subtracting the

inorganic species from the total PM mass), as the slope of the regression between RM versus OC. Details on the calculation of the F_{OC-OM} can be found in the Supplement (section S5). In C-C, all seasonal regressions had $R^2 \geq 0.6$, indicating that the RM is related to the OC fraction and thus to OM. Fig. 6 shows the F_{OC-OM} seasonal variation from spring (1.43) < autumn (1.59) < summer (1.85) < winter (2.05), indicating a higher degree of OM oxidation during both winter and summer, which are probably linked to winter emissions of biomass burning and summer oxidation processes of organic compounds from biogenic origin. Both of these processes are known to be linked to high values of F_{OC-OM} (Simon et al., 2011; Xing et al., 2013) reinforcing the hypothesis of the seasonal variation of the combustion factor. A F_{OC-OM} value of 2.1 is the commonly accepted value for rural sites according to the findings of Turpin and Lim (2001), however in the C-C site only the winter average was similar while the other seasonal averages were up to 30% lower and variable according to the seasonality of the sources and the local processes affecting the degree of oxidation of the carbonaceous aerosols.

The contribution of the combustion factor over $PM_{2.5}$ mass in C-C is in the same range of concentrations found for the combustion sources in other PMF studies conducted on urban and suburban sites in Northern France. Bressi et al. (2014) identified 3 combustion sources in Paris: biomass burning ($1.8 \mu g m^{-3}$, 12% of total $PM_{2.5}$), road traffic ($2.1 \mu g m^{-3}$, 14%) and heavy oil combustion ($2.4 \mu g m^{-3}$, 16%), while Roig Rodelas (2018) identified in Douai biomass burning ($1.6 \mu g m^{-3}$, 12%) and road traffic ($0.8 \mu g m^{-3}$, 6%) combustion sources. Both studies agreed on the important increase of the biomass burning source during winter, and its disappearance in summer. When comparing the sum of the identified combustion sources in Paris ($6.32 \mu g m^{-3}$, 42%) and Douai ($2.4 \mu g m^{-3}$, 18%), it was surprising to find that the combustion source levels in the rural site of C-C ($4.6 \mu g m^{-3}$, 40.2%) were in the same range as these cities. Moreover, the annual average levels of OC and EC in Paris at different site typologies ranged between 2.1 and 3.2 ± 1.5 – $2.5 \mu g OC m^{-3}$ and 0.4 – 1.4 ± 0.3 – $0.7 \mu g EC m^{-3}$ (Bressi et al., 2013), within range from to the levels found in C-C ($2.5 \pm 2.2 \mu g OC m^{-3}$ and $0.4 \pm 0.5 \mu g EC m^{-3}$). Additionally, the annual levels and daily variability of EC were found to be almost identical to the results of BC in the study of (Roig Rodelas et al., 2019b), ranging in between 0.4 and $0.9 \mu g m^{-3}$ on an annual basis and displaying two peaks, one in the morning and one on the evening. Although there may be some differences due to the temporal gap between campaigns, these similarities point to a strong regional background of combustion-based aerosols in the North of

France. This assumption is consistent with the rather diffuse geographical origin of the organic aerosols in C-C (NWR plots of the RM in Fig. 6).

4.2. Nitrate rich

The NO_3 -rich source factor is, alongside the SO_4 -rich factor, one of the main major drivers of $PM_{2.5}$ in the North of France (Bressi et al., 2013; Putaud et al., 2010; Roig Rodelas et al., 2019b). The main species in this factor is NH_4NO_3 (Fig. 3b), as the NH_4^+/NO_3^- molar ratio is 0.88, close to the value of 1 expected for NH_4NO_3 . The presence of EC in the factor suggests that there may be combustion contributions towards this factor (Fraser et al., 1998). NH_4NO_3 formation depends on NH_3 , emitted mostly by agricultural sources, and HNO_3 , a secondary species which has different formation pathways depending on its daytime chemistry (Reaction 1–2, (Calvert and Stockwell, 1983) or night-time chemistry (Reactions 3–5, Pathak et al., 2009; Brown and Stutz, 2012). The annual diel profile of HNO_3 suggests that both daytime and night-time formation of occur (Fig. 7a), although in a limited rate compared to the high pool of NO, HONO and NO_2 available (Fig. 7b).



NH_4NO_3 is involved in an equilibrium with its precursor gases NH_3 and HNO_3 (Reaction 2), and this depends on ambient temperature and RH. At high temperatures and dry conditions, the equilibrium is displaced towards the gas phase, while humid and cold conditions favour the aerosol formation (Seinfeld and Pandis, 2016). This contributes to the higher concentrations of the NO_3 -rich factor during autumn and spring, when the cool temperatures and high RH along with the fertilization events of the agricultural fields enhance NH_4NO_3 concentrations (Fig. 5b). On the contrary, in summer, the warm and dry conditions displace the equilibrium towards the gas phase. During winter, even though the conditions are cold and humid, the daily seasonal profile flatlines as the weaker photochemical activity and the prohibition to

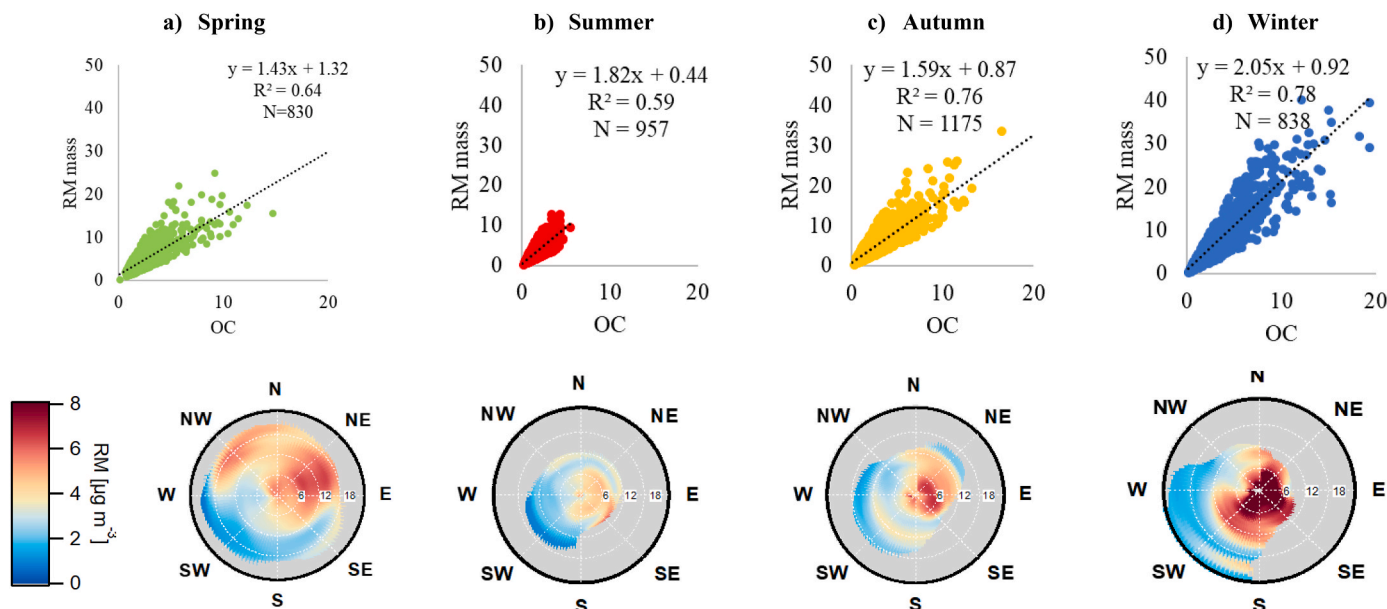


Fig. 6. Top: F_{OC-OM} estimation as the slope of the linear regression between OC and RM. Bottom: NWR plots of the RM used for determining the F_{OC-OM} .

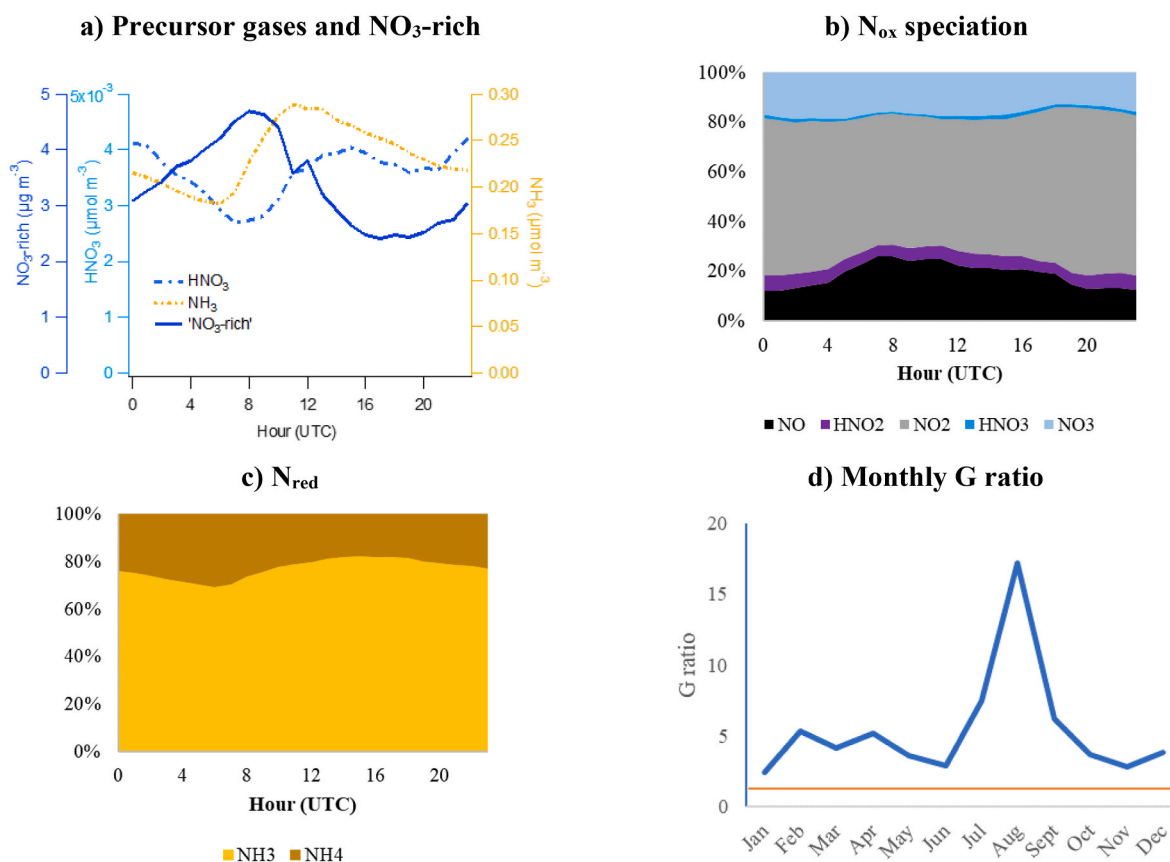


Fig. 7. (a) Diel annual profiles of HNO₃ and NH₃ (in $\mu\text{mol m}^{-3}$) and the NO₃-rich PMF factor (in $\mu\text{g m}^{-3}$); annual diel speciation of (b) oxidized nitrogen (N_{ox}) species and (c) reduced nitrogen (N_{red}) species; (d) monthly profile of the G ratio (the orange line corresponds to the limit between HNO₃ and NH₃ limited regimes).

apply fertilizers during the months of winter decrease the formation of HNO₃ and the additional inputs of NH₄NO₃, respectively (UE, 1991). The seasonality of the NO₃-rich source has been observed in other Northern French studies that concluded that this source was affected by transport processes from Benelux and Western Germany regardless of the site typology and PM fraction. Further discussion will be presented in Section 4.5.

This equilibrium also explains the daily variations of this factor (Fig. 7a), as the NO₃-rich concentrations increase during night-time, peaking between 6:00–9:00 UTC, while reaching their minimum in the afternoon. Indeed, the lowest air temperature of the day occurs just before sunrise, thus favouring the condensation of dew on aerosol surfaces and the subsequent night-time heterogeneous aqueous reactions forming nitrate (Reactions 4–5). This phenomenon may go on at sunrise when the soil moisture evaporates and saturates the air layer just above ground. As NH₃ is highly soluble in water, it is likely that part of NH₃ solubilizes in the morning dew, thus explaining the minimum (respectively maximum) observed in the diel variation of NH₃ (respectively NH₄⁺) in Fig. 7c.

To better understand the processes ongoing with the NH₄NO₃, the speciation of the oxidized N (N_{ox}) species (NO, HONO, NO₂, HNO₃ and NO₃⁻), reduced N species (NH₃ and NH₄⁺) and the gas ratio (G), which expresses the ratio between free NH₃ and total nitrate after neutralizing all H₂SO₄ (Ansari and Pandis, 1999, Equation (1)), all concentrations expressed as $\mu\text{mol m}^{-3}$. If the ratio is below 1 there is a NH₃-limited regime, while above 1 value indicates HNO₃-limited regime.

$$G = \frac{\text{NH}_3 + \text{NH}_4^+ - 2\text{SO}_4^{2-}}{\text{HNO}_3 + \text{NO}_3^-} \quad (1)$$

In the rural site of C–C, it was likely that the chemical regime was HNO₃-limited as the levels of NH₃ are always high enough to neutralize any

acid species. The annual NH₃ molar concentrations were sixty times higher than HNO₃ and thus NH₃, which accounts for $\geq 70\%$ of the reduced N on an annual basis (Fig. 7c), would quickly neutralize HNO₃ whenever is available. This is further supported by the G ratio, which is well above 1 all over the year (Fig. 7d). According to Ren et al. (2021), when there is significantly free NH₃ available to react with HNO₃, it decreases the dry deposition of HNO₃ and increases the lifetime of the NO₃-rich particles in the atmosphere and thus their regional transport (as explained in Section 4.5).

Interestingly, the formation of HNO₃ depends on the availability of NO₂ but also on the oxidizing capacity of the atmosphere. This was demonstrated during the first COVID-19 lockdown periods. In France in spring 2020, the decrease in NO_x emissions in the Parisian area brought as a result a significant decrease in the NO₃⁻ contribution towards PM₁, even though occasional long-range transport events supplied additional NO₃⁻ particles (Petit et al., 2021). In China, Ren et al. (2021) observed equal or even higher NO₃⁻ levels even NO_x decreased significantly due to the lockdown. They explained this as a result of increased O₃ production due to relaxed OH depletion and NO_x titration (Leung et al., 2020) that increased the oxidizing capability of the atmosphere and subsequently made more efficient the NO_x oxidation into HNO₃ and N₂O₅ species despite the emission decrease. These findings made imperative to target not only NO_x and NH₃ emissions, but also O₃ and the atmospheric oxidative capacity in order to decrease effectively secondary nitrate pollution.

4.3. Sulfate rich

The SO₄-rich factor accounts for 18% of the annual PM_{2.5} mass. Large seasonal variability is observed passing from 9.8% observed in winter to 26.5% during summer. (NH₄)₂SO₄ is formed when H₂SO₄ coming from

the SO₂ oxidation is neutralized with the NH₃ deriving from agricultural sources (Seinfeld and Pandis, 2016) and is stable regardless of the environmental temperature, effectively making the contribution towards PM_{2.5} of the SO₄-rich source (26.6%) almost as equal as the NO₃-rich source (27.5%) during summer. Fig. 5c shows the slow increase in concentrations until midday, and then decreases to a minimum during night-time for all seasons but winter, when the profile flatlines. Summer season was characterized by high temperatures, very high levels of O₃ and long insolation periods which enhanced the photochemical oxidation of SO₂ into SO₄²⁻ (Table 1).

The factor is driven by SO₄²⁻ and NH₄⁺ and their molar ratio is equal to 2.7, over the representative value of 2 for (NH₄)₂SO₄ (Fig. 3c) This indicated the presence of other sources of sulfate than pure (NH₄)₂SO₄. The small amounts of Cl⁻, K⁺ and OC point to the influence of biomass burning processes and secondary organic sources. Species such as KCl, K₂SO₄ and KNO₃ can appear in the fresh smoke coming from biomass burning (Li et al., 2003), potentially explaining the presence of K⁺ and Cl⁻ in this factor. Bressi et al. (2014) found in Paris high amounts of K⁺ and OM in the sulfate-rich factor that were attributed to a mixture of anthropogenic and biogenic sources (Hettiyadura et al., 2017). The presence of OC can be further explained as the aerosol component (NH₄)₂SO₄ has a high specific surface area and is acidic, properties that are known to enhance SOA formation by acting as a condensation surface for organic substances (Amato et al., 2009). Roig Rodelas (2018) observed that (NH₄)₂SO₄ only accounted for 33% of the mass of the sulfate-rich factor impacting the suburban site of Douai, implying that OM, although not measured in that study, was also present in this factor as indicated by the high species contribution of oxalate, which is a common tracer of secondary processes. As C-C is located between Paris and Douai, the presence of OC in the sulfate-rich factor, especially during summer seems consistent.

4.4. Mixed aged marine

The mass contribution of the MAM factor accounts for 15 % of the total PM_{2.5} mass. Even though the constraint on the PMF solution allowed to pinpoint the marine tracers, the sum of the marine tracers only accounts for 7% of the MAM factor mass, while the rest is accounted by NO₃⁻, SO₄²⁻ and OC. This may happen either by these components getting originated in polluted marine environments such as industrialized harbours of the North Sea or the Channel area with a high impact from maritime traffic (emitting NO_x, SO₂ and VOCs), or by the enrichment with anthropogenic pollutants as the fresh marine air masses pass over the polluted and densely-populated areas of Benelux and Paris metropolitan area and become aged. The diel temporal variation of this factor is flat suggesting no contribution of any local source or process to this factor. The monthly temporal variation shows higher contributions of this factor from March to July (Fig. 5d) probably linked to the higher frequency of winds coming from the North Sea sector in this period. The marine origins of this MAM source factor will be further highlighted in Section 4.5.

4.5. Geographical origin of the sources

4.5.1. Cluster analysis

To determine the influence of the origin and transport processes over PM_{2.5} concentrations, a cluster analysis was applied to the annual database. Fig. 8 shows four identified clusters from the 72-h back trajectories extracted every 12 h, with a total number of 727 back trajectories analyzed. The identified clusters are, by descending order of concentration: Continental (36% of frequency, 17.7 μg m⁻³), North Sea (9%, 13.4 μg m⁻³), France (24%, 13 μg m⁻³) and Atlantic Ocean (31%, 6.8 μg m⁻³). The North Sea, Atlantic Ocean and Continental clusters have a medium length, indicating the moderate wind speed associated to these air masses. On the contrary, the France cluster is short, meaning that the average speed of these air masses is slow, allowing the

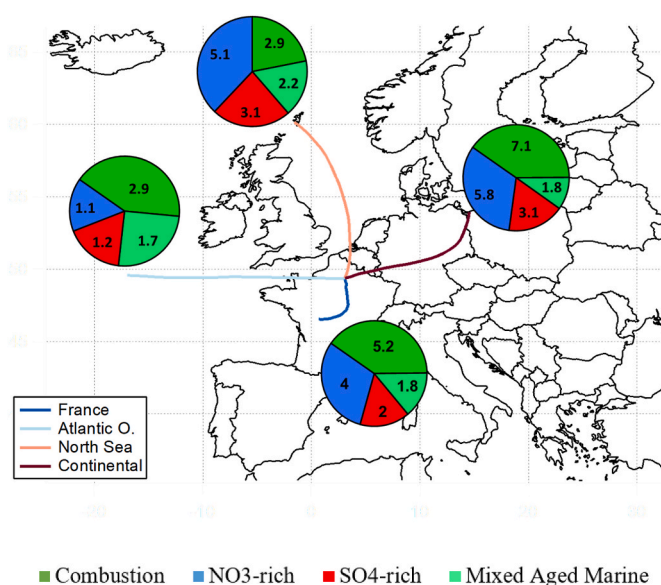


Fig. 8. Cluster analysis of the 1-year campaign in C-C. The pie charts represent the average composition of the PM_{2.5} for each cluster; concentrations expressed in μg m⁻³.

accumulation of pollutants while travelling towards our site.

The SIA-related sources are linked to the Continental and North Sea clusters and represent on average > 50% of the PM_{2.5} mass. In between these clusters is located Benelux, an area known to be heavily populated and industrialized, thus being a hotspot for NO_x, NH₃ and on a minor scale, SO₂ (Pay et al., 2012). These precursor gases may react while being transported from their source origin to arrive as particulate nitrate and sulfate to C-C. The North Sea cluster has the highest contribution of the MAM factor compared to the other clusters. The combustion factor alongside the NO₃-rich factor dominate both the Continent and the France clusters, representing the influence of transboundary and national combustion and agricultural sources. A more detailed vision on the potential geographical origins of each source is given in the next section.

4.5.2. NWR and PSCF analysis

Combustion factor: The NWR plot and PSCF map for the combustion factor display both strong local and transported signals (Fig. 9a). As discussed in Section 4.1, household heating using biomass as fuel is common in the surrounding houses and villages of C-C and may be responsible for the local signal, as seen in the winter NWR (Fig. S8a). This is consistent with the NWR plots of NO, NO₂, OC, EC, and K⁺ (Figs. S9–S11) and the NWR plots of RM (Fig. 7), showing high local concentrations associated to low wind speed ≤ 10 km h⁻¹, especially during winter where the heating necessities are at their peak. High average contributions (around 6 μg m⁻³) coming from the NE-SE sector are associated with faster wind speeds (≥ 14 km h⁻¹), potentially linked to population urban centres such as Saint Quentin (20 km NE) or Chauny-Tergnier (6 km SE). As regards the transported signal, the PSCF map (Fig. 9a) shows that the highest probability of high combustion contribution events would be originating from the French Grand Est region (40%) and on a lesser scale, Western Germany (20%), agreeing with previous PSCF analyses conducted in HdF (Golly et al., 2019; Waked et al., 2014).

NO₃-rich factor: The NWR shows a slight local signal of NH₄NO₃ (Fig. 9b). It is unclear if this comes from local formation or rather transported sources that partition into particle phase when they are in the surroundings of the measuring site, due to the semi volatile nature of this species and the ubiquitousness of NH₃ (Fig. S9g). As mentioned in Section 4.2, NO₃-rich particles from Benelux and Eastern Germany to the

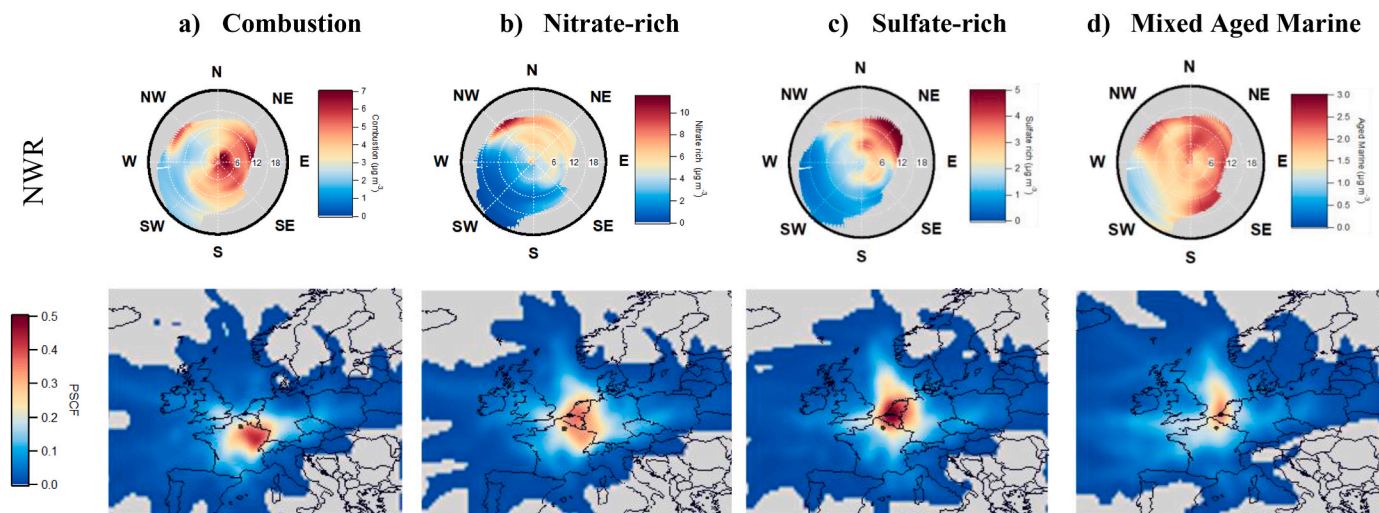


Fig. 9. Annual NWR and PSCF maps of the PMF sources.

north of France have been observed in other studies (Petit et al., 2017a; Roig Rodelas, 2018; Waked et al., 2014). In C-C, high contributions ($\geq 12 \mu\text{g m}^{-3}$) appeared from the NW associated to fast wind speeds ($\geq 15 \text{ km h}^{-1}$), highlighting the contribution of LRT over this factor, especially during spring (Fig. S8b). There are also contributions from the NE, although the concentrations are not as high ($\approx 8 \mu\text{g m}^{-3}$).

The PSCF map of the NO_3 -rich factor agrees with the cluster analysis and the previous studies for this area, highlighting the Netherlands, Benelux countries and the Grand Est region as the main contributors to this factor (Bressi et al., 2014; Waked et al., 2014). From these results, it seems apparent that there is a North-to-South geographical gradient of NO_3 particles, with the origin being located in Netherlands, where very high concentrations of NO_3 -rich sources (between 41 and 48% of the $\text{PM}_{2.5}$) were observed especially in the rural sites, as a consequence of the very high NH_3 concentrations neutralizing immediately all acidic gases (Mooibroek et al., 2011; Weijers et al., 2011). These particles are then transported towards the Northern French sites, where lower levels were observed (Fig. S7). The main issue with the PMF studies is the temporal distortion between observations as NH_4NO_3 is highly dependent on the sampling and meteorological conditions. However, this trend seems consistent with the results of the PMF studies conducted in the North-western Europe area, where the concentrations of the nitrate-rich factor at the Netherlands sites are twice as high as the Northern French ones, following this pattern consistently regardless of the year, implying that this factor is mostly related to this transport rather than having local formation of NH_4NO_3 .

SO_4 -rich factor: The NWR plot shows high concentrations ($\geq 5 \mu\text{g m}^{-3}$) coming from NE direction associated to fast wind speeds ($\geq 15 \text{ km h}^{-1}$), indicating that this factor is clearly influenced by LRT from continental sources. The PSCF points out to Benelux as a frequent source (in between 40 and 50% probability) of these particles. (Fig. 9c). As the oxidation of SO_2 is slower compared to other precursor gases, it is possible to apply the PSCF on this gas, highlighting Germany as one of the main origins, most likely due to the use of coal as fuel for electricity power generation (Fig. S12c). Additional sources of the sulfate-rich factor could be deduced from the moderately high probabilities ($\leq 30\%$) that both SO_2 and SO_4^{2-} may be coming from the North Sea, explained by the maritime traffic and the biological emissions of methane sulfonic acid (MSA) during warm periods, increasing the SO_4^{2-} levels (Chen et al., 2012).

MAM factor: The NWR plot was not conclusive, suggesting a rather diffuse and distant geographical origin. On the contrary, the PSCF map clearly shows high probabilities from the North Sea (30%) and to a lesser degree, the Channel, and the near Atlantic Sea (15%), emphasizing the

marine origin of the factor (Fig. 9d). This is coincident with both Cl^- and Na^+ PSCF maps highlighting the Atlantic, the UK islands and the Channel, and additionally, for Cl^- , the main signal comes from the North Sea (Fig. S12d). In fact, it also may explain the enrichment in SO_4^{2-} of this factor, as the North Sea has significant maritime traffic and offshore oil platforms, and is a hotspot for algal blooms which produce high concentrations of DMS, a biogenic precursor of SO_2 , especially during spring and summer seasons (Uher, 2006). when the concentrations of SO_2 and SO_4^{2-} are at their highest in our site together with a higher wind frequency coming from the North sector.

4.6. Rural air quality and health

In this study, we observed an annual average and standard deviation of hourly $\text{PM}_{2.5}$ of $12.2 \pm 9.3 \mu\text{g m}^{-3}$. This value exceeded the current annual limit value of $10 \mu\text{g m}^{-3}$ established by the AQ European Directive, and the recommended value of $5 \mu\text{g m}^{-3}$ proposed by the WHO, indicating that the population living in this rural area was exposed to an excessive atmospheric particulate pollution in 2018. Even though $\text{PM}_{2.5}$ concentrations were lower compared to urban areas, this study reveals the high content of SIA and combustion-derived aerosols in rural $\text{PM}_{2.5}$. Zhang et al. (2020) confirmed the generalized residential biomass burning sources in winter across France, while Chebaicheb et al. (2023) estimated that the PM_{10} in Lille, 150 km N from C-C, was dominated by NO_3^- and organic components coming mostly from regional background rather than local city production. Hence it is not unreasonable to hypothesize that the ultrafine fraction in the agricultural areas in the North of France have the same typology, given the results of our study on $\text{PM}_{2.5}$. Current regulations favour the reduction of $\text{PM}_{2.5}$ mass concentrations, but they do not consider the fact that aerosols could be more loaded with species harmful to human health (Casse et al., 2013; Achilleos et al., 2017; Guo et al., 2023). To be effective, mitigation policies must take into account the composition of atmospheric particles in order to tackle their most harmful sources and ultimately reduce the adverse consequences of exposure to $\text{PM}_{2.5}$.

Multiple studies are dedicated to understanding the toxicity of particles based on their chemical composition (Campbell et al., 2021; Ito et al., 2013; Liu et al., 2021; Yang et al., 2019), but such a task is daunting due to the large differences in particle morphology, sources, ageing processes, and aerosol size when inhaled. It is not in the scope of this paper to review the toxicity studies for the aerosol components, but it is relevant to the results obtained in this study, given the high contents of SIA and combustion-related aerosols. SIA toxicity has been assessed both from laboratory assays and epidemiological studies, and when fully

neutralized they show little toxicity (Park et al., 2018). However, the toxic response increase when the pH decreases due to incomplete neutralization by alkaline compounds, leading to higher solubility of organic and metallic components, triggering respiratory effects (Kelly and Fussell, 2012). SIA toxicity is strongly linked to their size, with ultrafine particles triggering stronger biological cytotoxicity at low doses (Akhtar et al., 2014; Xiang et al., 2023). When breaking down the SIA into their components, ammonium toxicity has been found to be very weak compared to nitrate and sulfate (Park et al., 2018; Zhang et al., 2021). PM_{2.5} sulfate particles have statistically significant effects over increased gastric cancer occurrence (Weinmayr et al., 2018), and pulmonary function issues when associated with carbonaceous aerosols (Atkinson et al., 2015; Wu et al., 2013). Nitrate effects and toxicity are not well understood yet, although it is related to high toxic responses in the respiratory system and pneumonia cases in childhood (Xiang et al., 2023). Combustion-based aerosols have been stated to be more toxic compared to non-combustion ones due to the huge heterogeneity of organic species contained within them, including polyaromatic hydrocarbons (PAH), quinones, and heavy metals associated (Park et al., 2018; Xia et al., 2004). As for EC toxicity, Atkinson et al. (2015) found a 1.3% increase in all-cause mortality per 1 µg m⁻³ increase in EC, considering that EC particles may be a carrier medium for other toxic components (heavy metals and organic components such as PAH).

The mixture of local and transported combustion aerosols, and the strong regional background supplying SIA aerosols may be more harmful for the human health of the people living in rural environments than initial estimates. Further research must be conducted in order to assess the effects of the combination of the SIA and combustion-based aerosols on human health.

5. Conclusions

For the first time at a rural site in the North of France, one year of continuous high time resolution measurements was collected using a MARGA, an OCEC semi-continuous analyzer, a TEOM-FDMS and NO_x, GC-FID and O₃ gas analyzers. This allowed for the characterization of gas precursors and PM_{2.5} speciation in various chemistry and meteorological conditions. The PM_{2.5} mass was dominated by SIA and OM, accounting for 51% and 33% of annual PM_{2.5} mass, respectively. Four p. m._{2.5} sources were identified using PMF analysis: combustion, nitrate-rich, sulfate-rich, and mixed aged marine. The combustion factor is the major single source, contributing 40.2% of the PM_{2.5} mass. It is mostly linked to local biomass burning for heating during the cold periods. Yet transport events of combustion aerosols from the continental platform and Grand Est region occur, especially during winter and spring. During the summer, biogenic secondary organic aerosols and eventual agricultural waste events were suspected to contribute to this factor. Surprisingly, the levels of the combustion factor mass contributions at the C-C site are comparable to the ones found in other Northern French PMF studies, even though they were conducted in heavier anthropogenic environments. This suggests that the region is subjected to a strong regional background influence of combustion-related particles. The contribution of both the NO₃-rich and SO₄-rich factors accounts for 44.8% of the PM_{2.5} mass, indicating that SIA-related particles are the main drivers of PM_{2.5} variability. NH₄NO₃ was the dominant component throughout the year except during the summer when (NH₄)₂SO₄ was equally significant (23%). The NO₃-rich factor temporal variability depends on the thermodynamic equilibrium between the particle and precursor gas phases, related to air temperature and RH. Aside from the meteorological conditions, the local formation of secondary nitrate in the C-C site is limited by the availability of HNO₃ since the chemical regime remains NH₃-rich throughout the year. In fact, although NO₂ is available, little HNO₃ is formed both by daytime and night-time radical chemistries due to the rather low atmospheric oxidative capacity. The highest concentrations of NO₃ originate from Netherlands, Belgium and the French Grand Est region, and are observed during the agricultural

fertilization months. The sources of particulate SO₄ are related to transport processes from the Benelux/Germany areas due to industrial activities (sulfate-rich factor) and the North Sea probably due to maritime traffic (mixed aged marine factor). Although PM_{2.5} concentrations are lower in rural areas compared to urban sites, episodes of high concentrations may be frequent. This study emphasizes the high contributions of regionally transported combustion aerosols and SIA linked to anthropogenic activities to relatively cleaner rural sites. Therefore, reducing particulate pollution in rural areas in the north of France requires concerted transnational action to reduce emissions from agriculture and combustion (biomass for heating and fossil fuels for maritime and road traffic). The oxidizing capacity of the atmosphere is another issue to consider. Finally, few studies exist on the effect on human health of co-exposure to a mixture of combustion aerosols and SIA, so this subject remains to be explored.

Funding sources

Pablo Espina Martin PhD grant was supported by the Hauts-de-France Regional Council and the CPER CLIMBIO and ECRIN projects funded by the Région Hauts-de-France, the French Ministry of Education and Research and the European Regional Development Fund (ERDF), and the CaPPA project funded by ANR through the PIA under contract ANR-11-LABX-0005-01.

CRediT authorship contribution statement

P. Espina-Martin: Writing – original draft, Visualization, Validation, Software, Methodology, Investigation, Formal analysis, Data curation, Conceptualization. **E. Perdrix:** Writing – review & editing, Validation, Supervision, Software, Resources, Project administration, Methodology, Investigation, Funding acquisition, Formal analysis, Data curation, Conceptualization. **L.Y. Alleman:** Writing – review & editing, Validation, Supervision, Software, Resources, Project administration, Methodology, Investigation, Funding acquisition, Formal analysis, Data curation, Conceptualization. **P. Coddeville:** Validation, Resources, Project administration, Funding acquisition, Conceptualization.

Declaration of competing interest

The authors declare that they have no known competing financial interests or personal relationships that could have appeared to influence the work reported in this paper.

Data availability

Data will be made available on request.

Acknowledgment

IMT Nord Europe acknowledges financial support from the Labex CaPPA project (ANR-11-LABX-0005-01), which is funded by the French National Research Agency (ANR) through the Programme d'Investissement d'Avenir (PIA), and the CPER CLIMBIO and CPER ECRIN, both financed by the Regional Council "Hauts-de-France" and the European Regional Development Fund (ERDF). We would like to thank the Région Hauts-de-France and IMT Nord Europe for funding the doctoral grant of Pablo Espina Martin, Benoit Rocq and Atmo Hauts-de-France for providing support and datasets of PM_{2.5} mass concentration, NO_x, O₃, and meteorological variables during the 1-year campaign.

Appendix A. Supplementary data

Supplementary data to this article can be found online at <https://doi.org/10.1016/j.atmosenv.2024.120660>.

References

- Achilleos, S., Kioumourtzoglou, M.-A., Wu, C.-D., Schwartz, J.D., Koutrakis, P., Papatheodorou, S.I., 2017. Acute effects of fine particulate matter constituents on mortality: a systematic review and meta-regression analysis. *Environ. Int.* 109, 89–100. <https://doi.org/10.1016/j.envint.2017.09.010>.
- Akhtar, U.S., Rastogi, N., McWhinney, R.D., Urch, B., Chow, C.-W., Evans, G.J., Scott, J. A., 2014. The combined effects of physicochemical properties of size-fractionated ambient particulate matter on in vitro toxicity in human A549 lung epithelial cells. *Toxicol Rep* 1, 145–156. <https://doi.org/10.1016/j.toxrep.2014.05.002>.
- Alleman, L.Y., Lamaison, L., Perdrix, E., Robache, A., Galloo, J.-C., 2010. PM10 metal concentrations and source identification using positive matrix factorization and wind sectoring in a French industrial zone. *Atmos. Res.* 96, 612–625. <https://doi.org/10.1016/j.atmosres.2010.02.008>.
- Amato, F., Pandolfi, M., Escrig, A., Querol, X., Alastuey, A., Pey, J., Perez, N., Hopke, P. K., 2009. Quantifying road dust resuspension in urban environment by Multilinear Engine: a comparison with PMF2. *Atmos. Environ.* 43, 2770–2780. <https://doi.org/10.1016/j.atmosenv.2009.02.039>.
- Andersen, Z.J., Wahlin, P., Raaschou-Nielsen, O., Scheike, T., Loft, S., 2007. Ambient particle source apportionment and daily hospital admissions among children and elderly in Copenhagen. *J. Expo. Sci. Environ. Epidemiol.* 17, 625–636. <https://doi.org/10.1038/sj.jes.7500546>.
- Ansari, A.S., Pandis, S.N., 1999. An analysis of four models predicting the partitioning of semivolatile inorganic aerosol components. *Aerosol. Sci. Technol.* 31, 129–153. <https://doi.org/10.1080/027868299304200>.
- Atkinson, R., Aschmann, S.M., 1993. Hydroxyl radical production from the gas-phase reactions of ozone with a series of alkenes under atmospheric conditions. *Environ. Sci. Technol.* 27, 1357–1363. <https://doi.org/10.1021/es00044a010>.
- Atkinson, R.W., Mills, I.C., Walton, H.A., Anderson, H.R., 2015. Fine particle components and health—a systematic review and meta-analysis of epidemiological time series studies of daily mortality and hospital admissions. *J. Expo. Sci. Environ. Epidemiol.* 25, 208–214. <https://doi.org/10.1038/jes.2014.63>.
- Aymoz, G., Mathé, F., 2007. Intégration des modules FDMS et RST | LCSQA. INERIS - mines Douai.
- Bauer, J.J., Yu, X.-Y., Cary, R., Laulainen, N., Berkowitz, C., 2009. Characterization of the sunset semi-continuous carbon aerosol analyzer. *J. Air Waste Manag. Assoc.* 59, 826–833. <https://doi.org/10.3155/1047-3289.59.7.826>.
- Bigi, A., Ghermandi, G., 2016. Trends and variability of atmospheric PM_{2.5} and PM_{10-2.5} concentration in the Po Valley, Italy. *Atmos. Chem. Phys.* 16, 15777–15788. <https://doi.org/10.5194/acp-16-15777-2016>.
- Birch, M.E., Cary, R.A., 1996. Elemental carbon-based method for monitoring occupational exposures to particulate diesel exhaust. *Aerosol. Sci. Technol.* 25, 221–241. <https://doi.org/10.1080/02786829608965393>.
- Bressi, M., Sciare, J., Gherzi, V., Bonnaire, N., Nicolas, J.B., Petit, J.-E., Moukhtar, S., Rosso, A., Mihalopoulos, N., Féron, A., 2013. A one-year comprehensive chemical characterisation of fine aerosol (PM_{2.5}) at urban, suburban and rural background sites in the region of Paris (France). *Atmos. Chem. Phys.* 13, 7825–7844. <https://doi.org/10.5194/acp-13-7825-2013>.
- Bressi, M., Sciare, J., Gherzi, V., Mihalopoulos, N., Petit, J.-E., Nicolas, J.B., Moukhtar, S., Rosso, A., Féron, A., Bonnaire, N., Poulakis, E., Theodosi, C., 2014. Sources and geographical origins of fine aerosols in Paris (France). *Atmos. Chem. Phys.* 14, 8813–8839. <https://doi.org/10.5194/acp-14-8813-2014>.
- Brown, S.S., Stutz, J., 2012. Nighttime radical observations and chemistry. *Chem. Soc. Rev.* 41, 6405–6447. <https://doi.org/10.1039/C2CS35181A>.
- Calvert, J.G., Stockwell, W.R., 1983. Acid generation in the troposphere by gas-phase chemistry. *Environ. Sci. Technol.* 17, 428A–443A. <https://doi.org/10.1021/es00115a727>.
- Campbell, S.J., Wolfer, K., Uttinger, B., Westwood, J., Zhang, Z.-H., Bukowiecki, N., Steimer, S.S., Vu, T.V., Xu, J., Straw, N., Thomson, S., Elzein, A., Sun, Y., Liu, D., Li, L., Fu, P., Lewis, A.C., Harrison, R.M., Bloss, W.J., Loh, M., Miller, M.R., Shi, Z., Kalberer, M., 2021. Atmospheric conditions and composition that influence PM_{2.5} oxidative potential in Beijing, China. *Atmos. Chem. Phys.* 21, 5549–5573. <https://doi.org/10.5194/acp-21-5549-2021>.
- Cassee, F.R., Héroux, M.-E., Gerlofs-Nijland, M.E., Kelly, F.J., 2013. Particulate matter beyond mass: recent health evidence on the role of fractions, chemical constituents and sources of emission. *Inhal. Toxicol.* 25, 802–812. <https://doi.org/10.3109/08958378.2013.850127>.
- Cavalli, F., Viana, M., Yttri, K.E., Genberg, J., Putaud, J.-P., 2010. Toward a standardised thermal-optical protocol for measuring atmospheric organic and elemental carbon: the EU-SAAR protocol. *Atmos. Meas. Tech.* 3, 79–89. <https://doi.org/10.5194/amt-3-79-2010>.
- Chebaicheb, H., de Brito, J.F., Chen, G., Tison, E., Marchand, C., Prévôt, A.S.H., Favez, O., Riffault, V., 2023. Investigation of four-year chemical composition and organic aerosol sources of submicron particles at the ATOLL site in northern France. *Environ. Pollut.* 330, 121805. <https://doi.org/10.1016/j.envpol.2023.121805>.
- Chen, L., Wang, J., Gao, Y., Xu, G., Yang, X., Lin, Q., Zhang, Y., 2012. Latitudinal distributions of atmospheric MSA and MSA/nss-SO₄²⁻ ratios in summer over the high latitude regions of the Southern and Northern Hemispheres. *J. Geophys. Res. Atmos.* 117. <https://doi.org/10.1029/2011JD016559>.
- Crenn, V., Chakraborty, A., Fronval, I., Petitprez, D., Riffault, V., 2018. Fine particles sampled at an urban background site and an industrialized coastal site in Northern France—Part 2: comparison of offline and online analyses for carbonaceous aerosols. *Aerosol. Sci. Technol.* 52, 287–299. <https://doi.org/10.1080/02786826.2017.1403008>.
- Crenn, V., Fronval, I., Petitprez, D., Riffault, V., 2017. Fine particles sampled at an urban background site and an industrialized coastal site in Northern France — Part 1: seasonal variations and chemical characterization. *Sci. Total Environ.* 578, 203–218. <https://doi.org/10.1016/j.scitotenv.2015.11.165>.
- Drüge, T., Nabat, P., Mallet, M., Somot, S., 2019. Model simulation of ammonium and nitrate aerosols distribution in the Euro-Mediterranean region and their radiative and climatic effects over 1979–2016. *Atmos. Chem. Phys.* 19, 3707–3731. <https://doi.org/10.5194/acp-19-3707-2019>.
- EEA, 2021. Air Quality in Europe 2021 [WWW Document]. URL: <https://www.eea.europa.eu/publications/air-quality-in-europe-2021/>, 8.25.22.
- Espina-Martin, P., Perdrix, E., Alleman, L.Y., Coddeville, P., 2022. Practical approach for an easy determination of the limit of detection and uncertainty budget associated with on-line measurements of gas and aerosols by ion chromatography. *Atmos. Environ.*, 119285. <https://doi.org/10.1016/j.atmosenv.2022.119285>.
- European Commission, 2019. Special Eurobarometer 497: Attitudes of Europeans towards Air Quality - Data Europa EU [WWW Document]. URL: https://data.europa.eu/data/datasets/s2239_92_1_497_eng?locale=en, 8.23.22.
- Fraser, M.P., Cass, G.R., Simoneit, B.R.T., 1998. Gas-phase and particle-phase organic compounds emitted from motor vehicle traffic in a Los Angeles roadway tunnel. *Environ. Sci. Technol.* 32, 2051–2060. <https://doi.org/10.1021/es970916e>.
- Gauss, M., Tsyro, S., Benedictow, A., Fagerli, H., Hjellbrekke, A.-G., Aas, W., Solberg, S., 2019. EMEP MSC-W Model Performance for Acidifying and Eutrophying Components, Photo-Oxidants and Particulate Matter in 2017 131.
- Golly, B., Waked, A., Weber, S., Samake, A., Jacob, V., Conil, S., Rangognio, J., Chretien, E., Vagnot, M.-P., Robic, P.-Y., Besombes, J.-L., Jaffrezo, J.-L., 2019. Organic markers and OC source apportionment for seasonal variations of PM_{2.5} at 5 rural sites in France. *Atmos. Environ.* 198, 142–157. <https://doi.org/10.1016/j.atmosenv.2018.10.027>.
- Guo, B., Huang, S., Li, S., Han, X., Lin, H., Li, Y., Qin, Z., Jiang, X., Wang, Z., Pan, Y., Zhang, J., Yin, J., Zhao, X., 2023. Long-term exposure to ambient PM_{2.5} and its constituents is associated with MAFLD. *JHEP Reports* 5, 100912. <https://doi.org/10.1016/j.jhepr.2023.100912>.
- Harrison, R.M., 2018. Urban atmospheric chemistry: a very special case for study. *npj Clim Atmos Sci* 1, 1–5. <https://doi.org/10.1038/s41612-017-0010-8>.
- Harrison, R.M., Yin, J., Tilling, R.M., Cai, X., Seakins, P.W., Hopkins, J.R., Lansley, D.L., Lewis, A.C., Hunter, M.C., Heard, D.E., Carpenter, L.J., Creasey, D.J., Lee, J.D., Pilling, M.J., Carslaw, N., Emmerson, K.M., Redington, A., Derwent, R.G., Ryall, D., Mills, G., Penkett, S.A., 2006. Measurement and modelling of air pollution and atmospheric chemistry in the U.K. West Midlands conurbation: overview of the PUMA Consortium project. *Sci. Total Environ.* 360, 5–25. <https://doi.org/10.1016/j.scitotenv.2005.08.053>.
- Hauglustaine, D.A., Balkanski, Y., Schulz, M., 2014. A global model simulation of present and future nitrate aerosols and their direct radiative forcing of climate. *Atmos. Chem. Phys.* 14, 11031–11063. <https://doi.org/10.5194/acp-14-11031-2014>.
- Heard, D.E., Carpenter, L.J., Creasey, D.J., Hopkins, J.R., Lee, J.D., Lewis, A.C., Pilling, M.J., Seakins, P.W., Carslaw, N., Emmerson, K.M., 2004. High levels of the hydroxyl radical in the winter urban troposphere. *Geophys. Res. Lett.* 31. <https://doi.org/10.1029/2004GL020544>.
- Henry, R., Norris, G.A., Vedantham, R., Turner, J.R., 2009. Source region identification using kernel smoothing. *Environ. Sci. Technol.* 43, 4090–4097. <https://doi.org/10.1021/es8011723>.
- Hettiyadura, A.P.S., Jayarathne, T., Baumann, K., Goldstein, A.H., Gouw, J.A. de, Koss, A., Keutsch, F.N., Skog, K., Stone, E.A., 2017. Qualitative and quantitative analysis of atmospheric organosulfates in Centreville, Alabama. *Atmos. Chem. Phys.* 17, 1343–1359. <https://doi.org/10.5194/acp-17-1343-2017>.
- INSEE, 2019. Populations légales 2019 – Commune de Caillouël-Crépigny (02139) | Insee [WWW Document]. URL: <https://www.insee.fr/fr/statistiques/6005800?geo=COM-02139>, 8.24.22.
- Ito, K., Ross, Z., Nadas, A., Lippman, T., 2013. Time series analysis of mortality, hospitalizations, and ambient PM_{2.5} and its components. In: *National Particle Component Toxicity (NPACT) Initiative: Integrated Epidemiologic and Toxicologic Studies of the Health Effects of Particulate Matter Components (Research No. 177)*. Health Effects Institute.
- Kelly, F.J., Fussell, J.C., 2012. Size, source and chemical composition as determinants of toxicity attributable to ambient particulate matter. *Atmos. Environ.* 60, 504–526. <https://doi.org/10.1016/j.atmosenv.2012.06.039>.
- Kim, S., Hong, K.-H., Jun, H., Park, Y.-J., Park, M., Sunwoo, Y., 2014. Effect of precipitation on air pollutant concentration in Seoul, Korea. *Asian Journal of Atmospheric Environment* 8, 202–211. <https://doi.org/10.5572/ajae.2014.8.4.202>.
- Kobza, J., Geremek, M., Dul, L., 2018. Characteristics of air quality and sources affecting high levels of PM₁₀ and PM_{2.5} in Poland, Upper Silesia urban area. *Environ. Monit. Assess.* 190, 515. <https://doi.org/10.1007/s10661-018-6797-x>.
- Koceva, M.M., Brandmüller, T., Lupu, I., Önnnerfors, Å., Corselli-Nordblad, L., Coyette, C., Johansson, A., Strandell, H., Wolff, P., Europäische Kommission (Eds.), 2016. *Urban Europe: Statistics on Cities, Towns and Suburbs, 2016 edition* Statistical Books/Eurostat. Publications Office of the European Union, Luxembourg.
- Ledoux, F., Kfoury, A., Delmaire, G., Roussel, G., El Zein, A., Courcot, D., 2017. Contributions of local and regional anthropogenic sources of metals in PM_{2.5} at an urban site in northern France. *Chemosphere* 181, 713–724. <https://doi.org/10.1016/j.chemosphere.2017.04.128>.
- Leung, D.M., Shi, H., Zhao, B., Wang, J., Ding, E.M., Gu, Y., Zheng, H., Chen, G., Liou, K.-N., Wang, S., Fast, J.D., Zheng, G., Jiang, J., Li, X., Jiang, J.H., 2020. Wintertime particulate matter decrease buffered by unfavorable chemical processes despite emissions reductions in China. *Geophys. Res. Lett.* 47, e2020GL087721. <https://doi.org/10.1029/2020GL087721>.
- Li, J., Pósfai, M., Hobbs, P.V., Buseck, P.R., 2003. Individual aerosol particles from biomass burning in southern Africa: 2, Compositions and aging of inorganic particles. *J. Geophys. Res. Atmos.* 108. <https://doi.org/10.1029/2002JD002310>.

- Lim, H.-J., Turpin, B.J., Edgerton, E., Hering, S.V., Allen, G., Maring, H., Solomon, P., 2003. Semicontinuous aerosol carbon measurements: comparison of Atlanta Supersite measurements. *J. Geophys. Res. Atmos.* 108 <https://doi.org/10.1029/2001JD001214>.
- Liu, L., Zhang, Yuanyuan, Yang, Z., Luo, S., Zhang, Yunquan, 2021. Long-term exposure to fine particulate constituents and cardiovascular diseases in Chinese adults. *J. Hazard Mater.* 416, 126051 <https://doi.org/10.1016/j.jhazmat.2021.126051>.
- Makkonen, U., Virkkula, A., Mäntykenttä, J., Hakola, H., Keronen, P., Vakkari, V., Aalto, P.P., 2012. Semi-continuous gas and inorganic aerosol measurements at a Finnish urban site: comparisons with filters, nitrogen in aerosol and gas phases, and aerosol acidity. *Atmos. Chem. Phys.* 12, 5617–5631. <https://doi.org/10.5194/acp-12-5617-2012>.
- Mbengue, S., Alleman, L.Y., Flament, P., 2014. Size-distributed metallic elements in submicronic and ultrafine atmospheric particles from urban and industrial areas in northern France. *Atmos. Res.* 135–136, 35–47. <https://doi.org/10.1016/j.atmosres.2013.08.010>.
- Mbengue, S., Fusek, M., Schwarz, J., Vodička, P., Šmejkalová, A.H., Holoubek, I., 2018. Four years of highly time resolved measurements of elemental and organic carbon at a rural background site in Central Europe. *Atmos. Environ.* 182, 335–346. <https://doi.org/10.1016/j.atmosenv.2018.03.056>.
- Meteo France, 2022. L'été | Météo-France [WWW Document]. URL <https://meteofrance.com/comprendre-la-meteo/saisons/ete>, 7.1.22.
- Mooibroek, D., Schaap, M., Weijers, E.P., Hoogerbrugge, R., 2011. Source apportionment and spatial variability of PM_{2.5} using measurements at five sites in The Netherlands. *Atmos. Environ.* 45, 4180–4191. <https://doi.org/10.1016/j.atmosenv.2011.05.017>.
- Norris, G., Duvall, R., Brown, S., Bai, S., 2014. Positive Matrix Factorization (PMF) 5.0 Fundamentals and User Guide 136.
- Paatero, P., Tapper, U., 1994. Positive matrix factorization: a non-negative factor model with optimal utilization of error estimates of data values. *Environmetrics* 5, 111–126. <https://doi.org/10.1002/env.3170050203>.
- Park, M., Joo, H.S., Lee, K., Jang, M., Kim, S.D., Kim, I., Borlaza, L.J.S., Lim, H., Shin, H., Chung, K.H., Choi, Y.-H., Park, S.G., Bae, M.-S., Lee, J., Song, H., Park, K., 2018. Differential toxicities of fine particulate matters from various sources. *Sci. Rep.* 8, 17007 <https://doi.org/10.1038/s41598-018-35398-0>.
- Pascal, M., Corso, M., Chanel, O., Declercq, C., Badaloni, C., Cesaroni, G., Henschel, S., Meister, K., Haluza, D., Martin-Olmedo, P., Medina, S., 2013. Assessing the public health impacts of urban air pollution in 25 European cities: results of the Aphekom project. *Sci. Total Environ.* 449, 390–400. <https://doi.org/10.1016/j.scitotenv.2013.01.077>.
- Pathak, R.K., Wu, W.S., Wang, T., 2009. Summertime PM_{2.5} ionic species in four major cities of China: nitrate formation in an ammonia-deficient atmosphere. *Atmos. Chem. Phys.* 9, 1711–1722. <https://doi.org/10.5194/acp-9-1711-2009>.
- Paulot, F., Jacob, D.J., Pinder, R.W., Bash, J.O., Travis, K., Henze, D.K., 2014. Ammonia emissions in the United States, European Union, and China derived by high-resolution inversion of ammonium wet deposition data: interpretation with a new agricultural emissions inventory (MASAGE NH3). *J. Geophys. Res. Atmos.* 119, 4343–4364. <https://doi.org/10.1002/2013JD021130>.
- Pay, M.T., Jiménez-Guerrero, P., Baldasano, J.M., 2012. Assessing sensitivity regimes of secondary inorganic aerosol formation in Europe with the CALIOPE-EU modeling system. *Atmos. Environ.* 51, 146–164. <https://doi.org/10.1016/j.atmosenv.2012.01.027>.
- Petit, J.-E., Amodeo, T., Meleux, F., Bessagnet, B., Menut, L., Grenier, D., Pellan, Y., Ockler, A., Rocq, B., Gros, V., Sciare, J., Favez, O., 2017a. Characterising an intense PM pollution episode in March 2015 in France from multi-site approach and near real time data: climatology, variabilities, geographical origins and model evaluation. *Atmos. Environ.* 155, 68–84. <https://doi.org/10.1016/j.atmosenv.2017.02.012>.
- Petit, J.-E., Dupont, J.-C., Favez, O., Gros, V., Zhang, Y., Sciare, J., Simon, L., Truong, F., Bonnaire, N., Amodeo, T., Vautard, R., Haeffelin, M., 2021. Response of atmospheric composition to COVID-19 lockdown measures during spring in the Paris region (France). *Atmos. Chem. Phys.* 21, 17167–17183. <https://doi.org/10.5194/acp-21-17167-2021>.
- Petit, J.-E., Favez, O., Albinet, A., Canonaco, F., 2017b. A user-friendly tool for comprehensive evaluation of the geographical origins of atmospheric pollution: wind and trajectory analyses. *Environ. Model. Software* 88, 183–187. <https://doi.org/10.1016/j.envsoft.2016.11.022>.
- Potier, E., Waked, A., Bourin, A., Minvielle, F., Péré, J.C., Perdrix, E., Michoud, V., Riffault, V., Alleman, L.Y., Sauvage, S., 2019. Characterizing the regional contribution to PM₁₀ pollution over northern France using two complementary approaches: chemistry transport and trajectory-based receptor models. *Atmos. Res.* 223, 1–14. <https://doi.org/10.1016/j.atmosres.2019.03.002>.
- Putaud, J.-P., Van Dingenen, R., Alastuey, A., Bauer, H., Birmili, W., Cyrys, J., Flentje, B., Fuzzi, S., Gehrig, R.C., Hansson, H.C., Harrison, R.M., Herrmann, H., Hiltnerberger, R., Hüglin, C., Jones, A.M., Kasper-Giebl, A., Kiss, G., Koussa, A., Kuhlbusch, T.A.J., Löschau, G., Maenhaut, W., Molnar, A., Moreno, T., Pekkanen, J., Perrino, C., Pitz, M., Puxbaum, H., Querol, X., Rodriguez, S., Salma, L., Schwarz, J., Smolik, J., Schneider, J., Spindler, G., ten Brink, H., Tursic, J., Viana, M., Wiedensohler, A., Raes, F., 2010. A European aerosol phenomenology – 3: physical and chemical characteristics of particulate matter from 60 rural, urban, and kerbside sites across Europe. *Atmos. Environ.* 44, 1308–1320. <https://doi.org/10.1016/j.atmosenv.2009.12.011>.
- Ren, C., Huang, X., Wang, Z., Sun, P., Chi, X., Ma, Y., Zhou, D., Huang, J., Xie, Y., Gao, J., Ding, A., 2021. Nonlinear response of nitrate to NO_x reduction in China during the COVID-19 pandemic. *Atmos. Environ.* 264, 118715 <https://doi.org/10.1016/j.atmosenv.2021.118715>.
- Roig Rodelas, R., 2018. Chemical Characterization, Sources and Origins of Secondary Inorganic Aerosols Measured at a Suburban Site in Northern France (Thesis). Lille 1.
- Roig Rodelas, R., Chakraborty, A., Perdrix, E., Tison, E., Riffault, V., 2019a. Real-time assessment of wintertime organic aerosol characteristics and sources at a suburban site in northern France. *Atmos. Environ.* 203, 48–61. <https://doi.org/10.1016/j.atmosenv.2019.01.035>.
- Roig Rodelas, R., Perdrix, E., Herbin, B., Riffault, V., 2019b. Characterization and variability of inorganic aerosols and their gaseous precursors at a suburban site in northern France over one year (2015–2016). *Atmos. Environ.* 200, 142–157. <https://doi.org/10.1016/j.atmosenv.2018.11.041>.
- Schaap, M., Otjes, R.P., Weijers, E.P., 2011. Illustrating the benefit of using hourly monitoring data on secondary inorganic aerosol and its precursors for model evaluation. *Atmos. Chem. Phys.* 11, 11041–11053. <https://doi.org/10.5194/acp-11-11041-2011>.
- Schauer, J.J., Lough, G.C., Shafer, M., Christensen, W., Arndt, M.F., DeMinter, J.T., Park, J.-S.P., 2006. Characterization of Metals Emitted from Motor Vehicles. Research No. 133).
- Schmid, H., Laskus, L., Jürgen Abraham, H., Baltensperger, U., Lavanchy, V., Bizjak, M., Burba, P., Cachier, H., Crow, D., Chow, J., Gnauk, T., Even, A., ten Brink, H.M., Giesen, K.-P., Hitznerberger, R., Hueglin, C., Maenhaut, W., Pio, C., Carvalho, A., Putaud, J.-P., Toom-Sauntry, D., Puxbaum, H., 2001. Results of the “carbon conference” international aerosol carbon round robin test stage I. *Atmos. Environ.* 35, 2111–2121. [https://doi.org/10.1016/S1352-2310\(00\)00493-3](https://doi.org/10.1016/S1352-2310(00)00493-3).
- Seinfeld, J.H., Pandis, S.N., 2016. In: Atmospheric Chemistry and Physics: from Air Pollution to Climate Change, third ed. Wiley.
- Simon, H., Bhawe, P.V., Swall, J.L., Frank, N.H., Malm, W.C., 2011. Determining the spatial and seasonal variability in OM/OC ratios across the US using multiple regression. *Atmos. Chem. Phys.* 11, 2933–2949. <https://doi.org/10.5194/acp-11-2933-2011>.
- Stein, A.F., Draxler, R.R., Rolph, G.D., Stunder, B.J.B., Cohen, M.D., Ngan, F., 2015. NOAA's HYSPLIT atmospheric transport and dispersion modeling system. *Bull. Am. Meteorol. Soc.* 96, 2059–2077. <https://doi.org/10.1175/BAMS-D-14-00110.1>.
- Thorpe, A., Harrison, R.M., 2008. Sources and properties of non-exhaust particulate matter from road traffic: a review. *Sci. Total Environ.* 400, 270–282. <https://doi.org/10.1016/j.scitotenv.2008.06.007>.
- Turpin, B.J., Lim, H.-J., 2001. Species contributions to PM_{2.5} mass concentrations: revisiting common assumptions for estimating organic mass. *Aerosol. Sci. Technol.* 35, 602–610. <https://doi.org/10.1080/02786820119445>.
- Twigg, M.M., Di Marco, C.F., Leeson, S., van Dijk, N., Jones, M.R., Leith, I.D., Morrison, E., Coyle, M., Proost, R., Peeters, A.N.M., Lemon, E., Frelink, T., Braban, C. F., Nemitz, E., Cape, J.N., 2015. Water soluble aerosols and gases at a UK background site – Part 1: controls of PM_{2.5} and PM₁₀ aerosol composition. *Atmos. Chem. Phys.* 15, 8131–8145. <https://doi.org/10.5194/acp-15-8131-2015>.
- UE, 1991. Directive 91/676/CEE du Conseil, du 12 décembre 1991, concernant la protection des eaux contre la pollution par les nitrates à partir de sources agricoles [WWW Document]. URL <https://eur-lex.europa.eu/legal-content/FR/ALL/?uri=CELEX%3A31991L0676>. (Accessed 19 September 2024).
- Uher, G., 2006. Distribution and air-sea exchange of reduced sulphur gases in European coastal waters. Estuarine, Coastal and Shelf Science, Trace gases in the European coastal zone 70, 338–360. <https://doi.org/10.1016/j.ecss.2006.05.050>.
- Ulbrich, I.M., Canagaratna, M.R., Zhang, Q., Worsnop, D.R., Jimenez, J.L., 2009. Interpretation of organic components from Positive Matrix Factorization of aerosol mass spectrometric data. *Atmos. Chem. Phys.* 9, 2891–2918. <https://doi.org/10.5194/acp-9-2891-2009>.
- Waked, A., Bourin, A., Michoud, V., Perdrix, E., Alleman, L.Y., Sauvage, S., Delaunay, T., Vermeesch, S., Petit, J.-E., Riffault, V., 2018. Investigation of the geographical origins of PM₁₀ based on long, medium and short-range air mass back-trajectories impacting Northern France during the period 2009–2013. *Atmos. Environ.* 193, 143–152. <https://doi.org/10.1016/j.atmosenv.2018.08.015>.
- Waked, A., Favez, O., Alleman, L.Y., Piot, C., Petit, J.-E., Delaunay, T., Verlinden, E., Golly, B., Besombes, J.-L., Jaffrezo, J.-L., Leoz-Garziandia, E., 2014. Source apportionment of PM₁₀ in a north-western Europe regional urban background site (Lens, France) using positive matrix factorization and including primary biogenic emissions. *Atmos. Chem. Phys.* 14, 3325–3346. <https://doi.org/10.5194/acp-14-3325-2014>.
- Waked, A., Sauvage, S., Borbon, A., Gauduin, J., Pallares, C., Vagnot, M.-P., Léonardis, T., Locoge, N., 2016. Multi-year levels and trends of non-methane hydrocarbon concentrations observed in ambient air in France. *Atmos. Environ.* 141, 263–275. <https://doi.org/10.1016/j.atmosenv.2016.06.059>.
- Weijers, E.P., Schaap, M., Nguyen, L., Matthijssen, J., Denier van der Gon, H.A.C., ten Brink, H.M., Hoogerbrugge, R., 2011. Anthropogenic and natural constituents in particulate matter in The Netherlands. *Atmos. Chem. Phys.* 11, 2281–2294. <https://doi.org/10.5194/acp-11-2281-2011>.
- Weinmayr, G., Pedersen, M., Stafoggia, M., Andersen, Z.J., Galassi, C., Munkenast, J., Jaensch, A., Oftedal, B., Krog, N.H., Aamodt, G., Pyko, A., Pershagen, G., Korek, M., De Faire, U., Pedersen, N.L., Östenson, C.-G., Rizzuto, D., Sørensen, M., Tjønneland, A., Bueno-de-Mesquita, B., Vermeulen, R., Eeftens, M., Concini, H., Lang, A., Wang, M., Tsai, M.-Y., Ricceri, F., Sacerdote, C., Ranzi, A., Cesaroni, G., Forastiere, F., de Hoogh, K., Beelen, R., Vineis, P., Kooter, I., Sokhi, R., Brunekreef, B., Hoek, G., Raaschou-Nielsen, O., Nagel, G., 2018. Particulate matter air pollution components and incidence of cancers of the stomach and the upper aerodigestive tract in the European Study of Cohorts of Air Pollution Effects (ESCAPE). *Environ. Int.* 120, 163–171. <https://doi.org/10.1016/j.envint.2018.07.030>.
- Wu, S., Deng, F., Hao, Y., Shima, M., Wang, X., Zheng, C., Wei, H., Lv, H., Lu, X., Huang, J., Qin, Y., Guo, X., 2013. Chemical constituents of fine particulate air pollution and pulmonary function in healthy adults: the Healthy Volunteer Natural

- Relocation study. *J. Hazard Mater.* 260, 183–191. <https://doi.org/10.1016/j.jhazmat.2013.05.018>.
- Xia, T., Korge, P., Weiss, J.N., Li, N., Venkatesen, M.I., Sioutas, C., Nel, A., 2004. Quinones and aromatic chemical compounds in particulate matter induce mitochondrial dysfunction: implications for ultrafine particle toxicity. *Environ. Health Perspect.* 112, 1347–1358. <https://doi.org/10.1289/ehp.7167>.
- Xiang, W., Wang, W., Du, L., Zhao, B., Liu, X., Zhang, X., Yao, L., Ge, M., 2023. Toxicological effects of secondary air pollutants. *Chem. Res. Chin. Univ.* 39, 326–341. <https://doi.org/10.1007/s40242-023-3050-0>.
- Xing, L., Fu, T.-M., Cao, J.J., Lee, S.C., Wang, G.H., Ho, K.F., Cheng, M.-C., You, C.-F., Wang, T.J., 2013. Seasonal and spatial variability of the OM/OC mass ratios and high regional correlation between oxalic acid and zinc in Chinese urban organic aerosols. *Atmos. Chem. Phys.* 13, 4307–4318. <https://doi.org/10.5194/acp-13-4307-2013>.
- Yang, Y., Ruan, Z., Wang, X., Yang, Y., Mason, T.G., Lin, H., Tian, L., 2019. Short-term and long-term exposures to fine particulate matter constituents and health: a systematic review and meta-analysis. *Environ. Pollut.* 247, 874–882. <https://doi.org/10.1016/j.envpol.2018.12.060>.
- Zhang, J., Cheng, H., Wang, D., Zhu, Y., Yang, C., Shen, Y., Yu, J., Li, Y., Xu, S., Zhang, S., Song, X., Zhou, Y., Chen, J., Jiang, J., Fan, L., Wang, C., Hao, K., 2021. Chronic exposure to PM2.5 nitrate, sulfate, and ammonium causes respiratory system impairments in mice. *Environ. Sci. Technol.* 55, 3081–3090. <https://doi.org/10.1021/acs.est.0c05814>.
- Zhang, Y., Albinet, A., Petit, J.-E., Jacob, V., Chevrier, F., Gille, G., Pontet, S., Chrétien, E., Dominik-Sègue, M., Levigoureux, G., Močnik, G., Gros, V., Jaffrezo, J.-L., Favez, O., 2020. Substantial brown carbon emissions from wintertime residential wood burning over France. *Sci. Total Environ.* 743, 140752 <https://doi.org/10.1016/j.scitotenv.2020.140752>.